Design and Analysis of Modified LLC Resonant Converter for Electric Vehicle Charging Infrastructure

A DISSERTATION

SUBMITTED IN PARTIAL FULFILLMENT OF THE REQUIREMENTS

FOR THE AWARD OF THE DEGREE

OF

MASTER OF TECHNOLOGY

IN

POWER ELECTRONICS AND SYSTEMS

Submitted by:

MONISH ANSARI

2K21/PES/10

Under the supervision of

PROF. MUKHTIAR SINGH

(Professor, EED, DTU)

MR. KULDEEP SINGH

(Assistant Professor, EED, DTU)

DEPARTMENT OF ELECTRICAL ENGINEERING

DELHI TECHNOLOGICAL UNIVERSITY

(Formerly Delhi College of Engineering)

Bawana Road, Delhi-110042

MAY, 2023

DEPARTMENT OF ELECTRICAL ENGINEERING

DELHI TECHNOLOGICAL UNIVERSITY

(Formerly Delhi College of Engineering)

Bawana Road, Delhi-110042

CANDIDATE'S DECLARATION

I, Monish Ansari, Roll No. 2K21/PES/10 student of MTech (Power Electronics & Systems), hereby declare that the project Dissertation titled **"Design and Analysis of Modified LLC Resonant Converter for Electric Vehicle Charging Infrastructure"** which is submitted by me to the Department of Electrical Engineering, Delhi Technological university, Delhi in partial fulfillment of the requirement for the award of the degree of Master of Technology, is original and not copied from any source without proper citation. This work has not previously formed the basis for the award of any Degree, Diploma Associateship, Fellowship, or other similar title or recognition.

Place: Delhi (Monish Ansari)

Date:

DEPARTMENT OF ELECTRICAL ENGINEERING

DELHI TECHNOLOGICAL UNIVERSITY

(Formerly Delhi College of Engineering)

Bawana Road, Delhi-110042

CERTIFICATE

I hereby certify that the project Dissertation titled **"Design and Analysis of Modified LLC Resonant Converter for Electric Vehicle Charging Infrastructure"** which is submitted by Monish Ansari, Roll No. 2K21/PES/10, Department of Electrical Engineering, Delhi Technological University, Delhi in partial fulfilment of the requirement for the award of the degree of Master of Technology, is a record of the project work carried out by the student under my supervision. To the best of my knowledge, this work has not been submitted in part or full for any Degree or Diploma to this University or elsewhere.

Place: Delhi
Date:

PROF. MUKHTIAR SINGH
(SUPERVISOR)

MR. KULDEEP SINGH
(CO-SUPERVISOR)

ABSTRACT

The design and analysis of Modified LLC Resonant Converter for a single-phase, two-stage On-Board charger (OBC) for a light load that may operate in the Grid to Vehicle (G2V) operation mode is presented in this thesis work. The first converter is controlled for this purpose using a Second Order Generalised Integrator (SOGI) control approach, which exhibits a stable steady state as well as excellent dynamic behaviour. The first stage AC-DC converter of an EV (Electric Vehicle) charger plays a very important role in supporting the grid power factor unity. To maintain the grid's power quality PQ at or above the international electrotechnical commission's (IEC)-61000-3-2 standard throughout operations. The efficacy of the design has also been confirmed under a variety of operational scenarios, including the occurrence of Sag and Swell grid voltage. The Modified LLC converter, which is utilized in the second stage of DC-DC conversion, may achieve Zero Voltage Switching (ZVS) for all switches. The modified LLC converter allows for substantially greater Voltage conversion while using fewer switches than a standard LLC converter, which substantially decreases reverse power and turn-off losses. Always using a discontinuous resonant current, the converter runs. To reduce the converter's initial inrush current, clamping diodes were included. To control the switches on the DC-DC converter, a proportional-integral controller is adopted. The battery voltage and charging current are monitored and managed by a PWM controller with a constant battery current. The 3.3kW system ratings are subjected to a thorough simulation investigation. An inductive load has also been linked to the grid to test the responsiveness of the grid.

DEPARTMENT OF ELECTRICAL ENGINEERING

DELHI TECHNOLOGICAL UNIVERSITY

(Formerly Delhi College of Engineering)

Bawana Road, Delhi-110042

ACKNOWLEDGEMENT

I would like to express my gratitude towards all the people who have contributed their precious time and effort to help me without whom it would not have been possible for me to understand and complete the project. I would like to thank Prof. Mukhtiar Singh, DTU Delhi, Department of Electrical Engineering, my Project Supervisor, for supporting, motivating, and encouraging me throughout this work was carried out. His readiness for consultation at all times, his educative comments, and his concern and assistance even with practical things have been invaluable.

Besides my supervisor, I would like to thank Mr. Kuldeep Singh, Department of Electrical Engineering, my Co-Supervisor, and all the Ph.D. scholars of PE LAB for helping me wherever required and providing me with continuous motivation during my research.

Finally, I must express my very profound gratitude to my parents, seniors, and my friends for providing me with unfailing support and continuous encouragement throughout the research work.

Date:

Monish Ansari
M.tech (Power Electronics & Systems)
Roll No. 2K21/PES/10

TABLE OF CONTENTS

LIST OF FIGURES

LIST OF TABLES

LIST OF ABBREVIATION

S. No.	Abbreviated Name	Full Name
1.	EV	Electric Vehicle
2.	ICE	Internal Combustion Engine
3.	BEV	Battery Electric Vehicle
4.	G2V	Grid to Vehicle
5.	V2G	Vehicle to Grid
6.	V2L	Vehicle to Load
7.	PHEV	Plug-in Hybrid Electric Vehicle
8.	OBC	On-Board Charger
9.	NGV	Natural Gas Vehicle
10.	DCFC	Direct Current Fast Charging
11.	ZVS	Zero Voltage Switching
12.	ZCS	Zero Current Switching
13.	DAB	Dual Active Bridge
14.	SR	Synchronous Rectifier
15.	SOGI	Second Order Generalized Integrator
16.	ISOP	Input Series Output Parallel
17.	CC	Constant Current
18.	CV	Constant Voltage
19.	PI	Proportional Integrator
20.	LPF	Low Pass Filter
21.	PWM	Pulse Width Modulation
22.	SoC	State of Charge
23.	THD	Total Harmonics Distortion
24.	FFT	Fast Fourier Transform
25.	VSC	Voltage Source Converter
26.	UPF	Unity Power Factor
27.	HCC	Hysteresis Current Control

LIST OF SYMBOLS

S. No.	Symbols	Description
1.	V_{in}	Input Voltage to the Converter
2.	L_r	Resonating Inductance
3.	L_m	Magnetizing Inductance
4.	f_s	Switching Frequency
5.	f_r	Resonating Frequency
6.	C_r	Resonating Capacitance
7.	C_o	Output Capacitance
8.	i_{Lm}	Magnetizing current
9.	i_s	Secondary current of the converter
10.	i_r	Resonating Current
11.	V_o	Output Voltage of Converter
12.	V_{dc}	DC Link Voltage
13.	R_{ac}	AC Resistance referred to primary of converter
14.	R_o	Actual output Resistance
15.	n	Number of turns
16.	Q	Quality Factor
17.	M	Gain of the Converter
18.	V_g, I_g	Grid Voltage, Grid Current
19.	R, L	Parallel Load Resistance and Inductance
20.	L_c	Input Side Filter Inductance
21.	ω	Angular Frequency of SOGI
22.	u_a	Unit template
23.	I_{bat}	Battery Current

Chapter 1

INTRODUCTION

The conversion to electric vehicles in the global transport network has picked up steam recently. Electric Vehicle (EV) charger consumption is rising in tandem with this development. Electric vehicle chargers are going to become a crucial component of the power system, highlighting the demand for effective charging methods.

1.1 BACKGROUND

The significant developments of electric cars and technological advancement are presenting new difficulties for the automobile industry [1], resulting in new demands for upcoming cars, as well as new, as of yet undiscovered transportation technologies. For instance, drivetrain modernization offers a more sustainable future, while self-driving vehicles will increase safety, accessibility, and effectiveness [2]. Though these changes also provide new cost frameworks and additional limitation requirements for vehicle improvement. When contrasted with automobiles powered by internal combustion engines (ICEs), BEVs' traction batteries add to the vehicle's weight [3] and cost. In addition, supplementary power usage and purchasing expenses are impacted by the sensors and processors in self-driving automobiles (AVs). The capacity of automobile manufacturers to develop future car ideas and guarantee their success in the automotive marketplace depends critically on their level of awareness of the latest developments and the costs associated with them.

Energy transport is a crucial component of the modern renewable energy future. By using EVs as a transport vector, it grows into a significant technology with a variety of uses. G2V (Grid to Vehicle) describes the concept that EV batteries are charged from the grid. Both a current source V2G (Vehicle to Grid) and a voltage source V2L (Vehicle to Load) may be created from the power that has been retained by battery packs for electric vehicles [4]–[5].

Vehicle-to-grid (V2G) has also drawn a lot of interest due to the rise of PHEVs and EVs that can serve as mobile storage units. Having the capacity to discharge battery

energy increases the flexibility of recharging batteries while also enabling stand-alone loads like rescue operations or exterior lighting. The need for a charger to utilize an EV's battery power to supply grid-connected loads or autonomous loads is expanding. Therefore, bidirectional operation, high power density, and reliability are crucial for the mobile offboard charger [6]. Compared to the upkeep and fuel expenses of conventional gasoline cars, the vehicle's upkeep expenses and the cost of the energy needed are significantly cheaper. As can be shown in Fig. 1.1, EVs have substantially less electricity cost per mile than conventional cars.

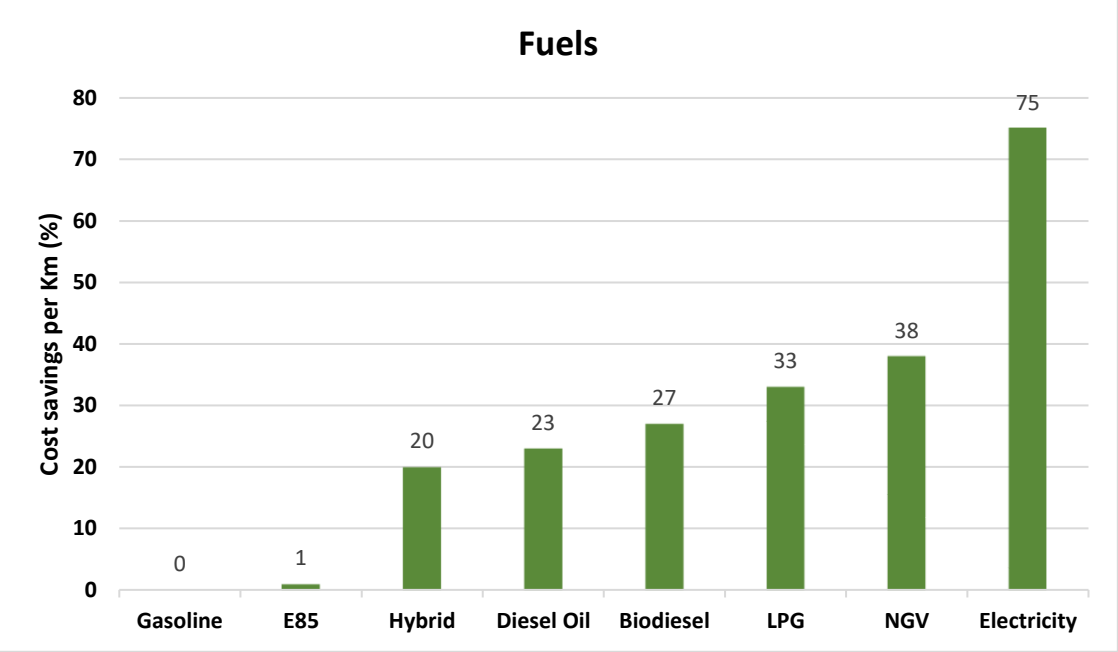

Fig. 1.1. Comparison of savings in cost per kilometer offered by vehicles.

1.2 Breakdown of infrastructure needed for charging electric vehicles: type, location, and speed

In general, the availability of charging stations is a crucial enabler for the implementation of EVs. A motorist's demands must be taken into account while choosing an EV recharging option because there are various speeds, prices, and places accessible. For lawmakers and market players to optimize the installation of charging infrastructure, the tactical importance of multiple charging modes, in specific household charging, voluntarily available charging, and charging at work, must be considered. In

this section, we provide details on the locations and methods of charging used by EV domestic clients.

1.3 Charging modes

The crispness of pricing extent varies greatly within academic, governmental, and commercial literature as well as between nations and regions. Here, we use the terms Level-1 (slow charging), Level-2 (slow to rapid charging utilizing AC), or Direct Current fast Charging (DCFC) to describe charging ratings. Charging modes 1 (slow), 2 (slow to semi-quick using AC), 3 (semi-fast to fast using AC), and 4 (DC fast charging) are described by a different rating system that is more often used in Europe. The high-level alignments of Levels I, II, DCFC, and the 4 charging modes is shown in Fig. 1.2 [7].

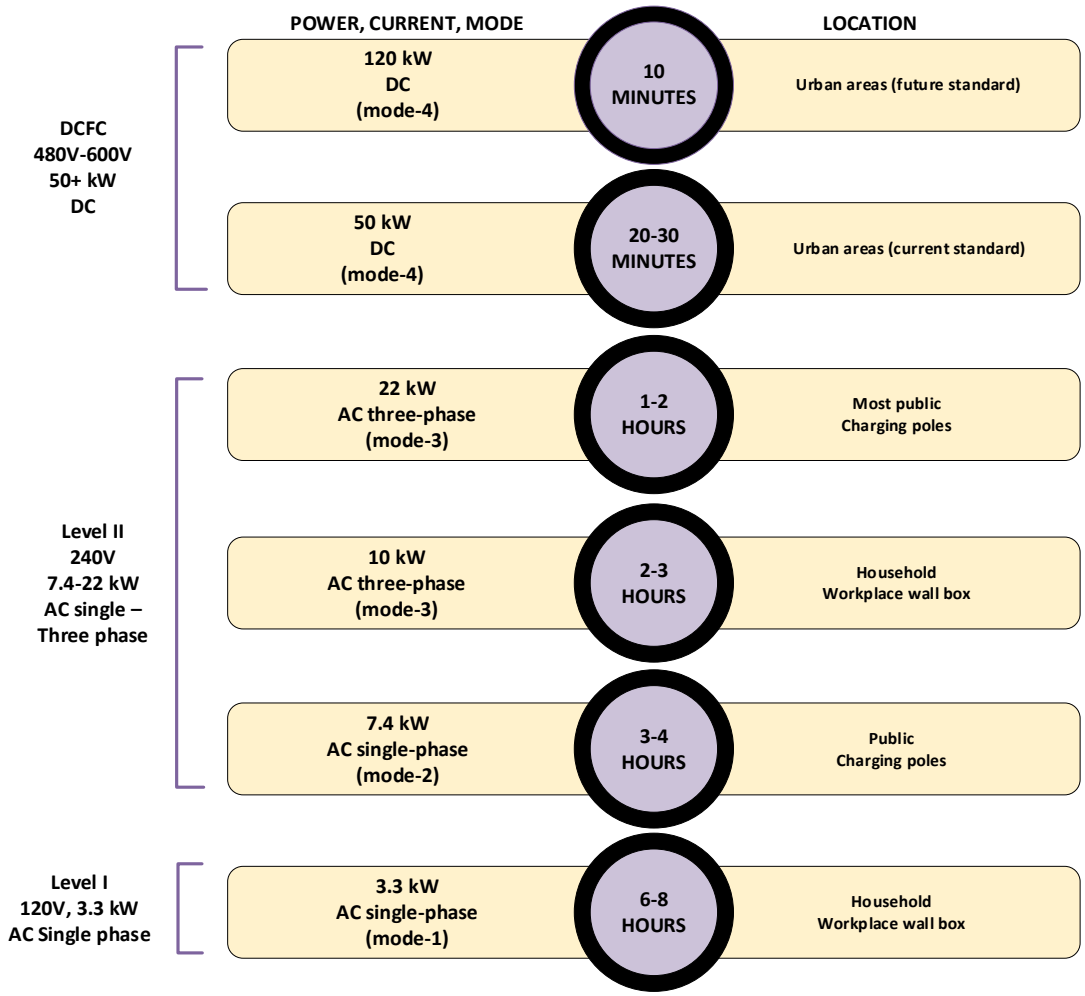

Fig. 1.2. Relative of charging ratings for a 100-kilometer driving distance.

1.4 Power Converters for Charging Stations

The LLC converter is frequently used for bidirectional power flow for various variable loads due to its soft switching characteristics. All agree that LLC converters have excellent efficiency, a compact size, and a wide range of zero voltage switching (ZVS) and zero current switchings (ZCS). For battery charging applications, LLC converters are being researched to attain high efficiency [8]. The most popular converter for these applications is the Dual Active Bridge (DAB) converter due to its automated power flow changes. Even yet, the benefit of an LLC resonant converter over a DAB converter remains obvious because of its superior soft-switching capabilities [9]. Figure (3) depicts the benefits of an LLC resonant converter.

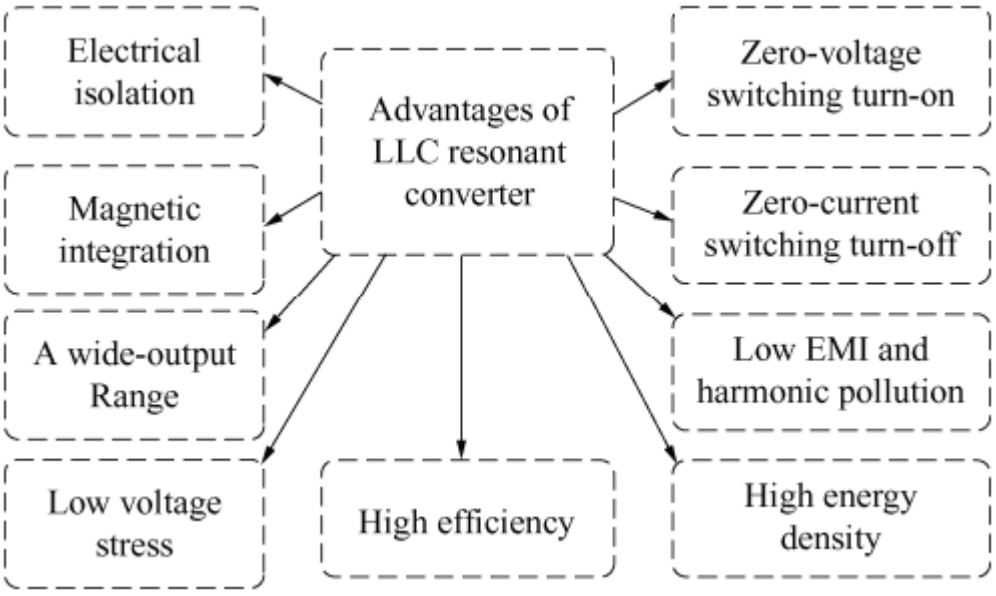

Fig. 1.3. Advantages of the LLC resonant converter

When learning LLC conversion, there are two obstacles to overcome. The first one is an asymmetrical structure which also increases the issues for the control strategy. The second is the present gentle start and protection. An asymmetrical two-resonant tank bidirectional CLLC converter is advantageous [10]-[11]. In both forward and reverse operations, the voltage gain is similar. However, the logic of control has to be changed to allow for bidirectional power flow. A bidirectional LC-type regulating method for LLC LC-type resonant converter was given in Paper [9]. Another way to look at it is

that the recommended [12] symmetrical design might also be made using an auxiliary inductor. Changing the switching frequency could automatically alter the direction of power flow. It is challenging to smoothly move between a variety of working modes, though. [13] described a bidirectional CLTC resonant converter with an extra resonant capacitor and an auxiliary transformer. These resonant converters' efficiency and dependability could decline if supplementary devices are added.

Because LLC resonant converters offer superior soft-switching capabilities in comparison to other converters for any load range, they are the optimal design for the dc-dc power conversion stage. [14]–[15]. A synchronous rectifier (SR) is frequently used to detect the current zero-crossing point or detect the device lowered voltage in order to achieve high conversion efficiency. These SR techniques are frequently used by LLC converters in unidirectional applications. However, as to the asymmetry of the configuration and gain characteristics, when working in bidirectional power applications, the SR must alternate in the middle of the two-side bridges. Sensing both power direction and changing control logic will make control plan more difficult.

1.5 Motivation

The major objective of this project is to comprehensively simulate and build an onboard battery charging system for electric cars using a Modified LLC resonant converter that can operate with a broad range of voltages while maintaining high efficiency. To lower the initial inrush current, the proposed DC-DC converter has been redesigned to employ fewer switches. The converter is examined in a grid with a broad voltage range. The Modified LLC converter is examined in various operating modes to create the best On-Board Charger. To achieve the necessary power factor under any circumstance, the input side SOGI controller is employed.

1.6 Outline

As stated previously, the primary goal of the thesis is to develop a battery charging system in G2V mode under variable grid conditions with the Modified LLC Resonant Converter. The presented work is as follows:

Chapter-1 This chapter provides the reader with an introduction to Electric Vehicle technology and background on the importance of isolated DC-DC converters with control structure to maintain grid reactivity and Battery parameters.

Chapter-2 In this chapter the Conventional LLC Half-Bridge is discussed with all the frequency ranges of Modulation.

Chapter-3 In this chapter the Modified LLC DC-DC converter is discussed with detailed study and modes of Operations.

Chapter-4 This chapter includes the ZVS analysis for the proposed Resonant converter. It also detailed the design and Frequency modulation for the LLC converter.

Chapter-5 SOGI Controller is described in this chapter with detailed analysis, which also covers the optimal input filter design for maintaining Grid stability.

Chapter-6 This chapter validates the results of the proposed system under variable conditions. Simulation results have been discussed.

Chapter-7 The study on the onboard battery charger for electric vehicles is summarised in this chapter, followed by information on the work's future direction.

Chapter 2

LLC RESONANT HALF-BRIDE POWER CONVERTER

2.1 OVERVIEW

Power-supply designs and their applications have been increasingly incorporating advancements in efficiency, power density, and component density. The growing interest in resonant power converters, including the adoption of higher switching frequencies and reduced switching losses, has reignited attention toward the utilization of LLC half-bridge configurations. The conventional LLC resonant converter distinguishes itself from conventional designs by employing frequency modulation instead of pulse-width modulation for power conversion, necessitating a unique design approach. However, the construction of such converters poses substantial challenges.

2.2 Resonant Converters: Review

A resonant circuit receives a square pulse of voltage or current created by the power switches. The output is supplied by tapping off some or all of the energy that the resonant circuit generated. The two basic types of resonant converters are the SRC, depicted in Figure 2.1(a), and the parallel resonant converter (PRC), depicted in Figure 2.1(b). The two of these converters adjust the driving voltage's frequency, which changes the resonant circuit's impedance, to modify the output voltage. The input voltage is break between this impedance and the load. Since an SRC acts as a voltage divider among the input and the load, its DC gain is limited to 1. It is difficult to manage the output while the load is low because to do so, the frequency must increase as the load decreases. It is so because the load's impedance is much higher than the impedance of the resonant circuit. Even at low loads, a sizable frequency variation is required for controlling the output when the input voltage spectrum is wide. In the PRC shown in Fig. 2.1(b), the load is attached in parallel with the resonant circuit, obtaining a sizable amount of flowing current. As a consequence, it is challenging to use parallel resonant configurations in settings with large amounts of power or significant load changes.

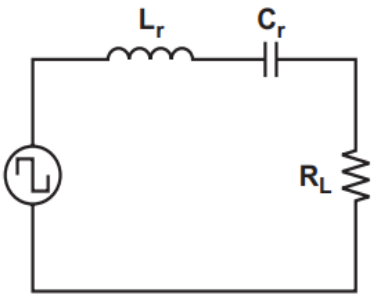

(a)

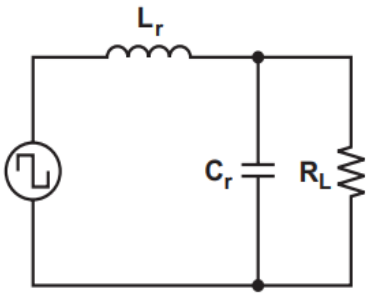

(b)

Fig. 2.1 Basic resonant-converter configurations. (a) Series. (b) parallel.

2.3 HALF-BRIDGE LLC RESONANT CONVERTER

This subsection describes the operation of a conventional isolated LLC resonant half-bridge converter along with a circuit design that has been simplified and the voltage-gain function, which connects input and output voltage.

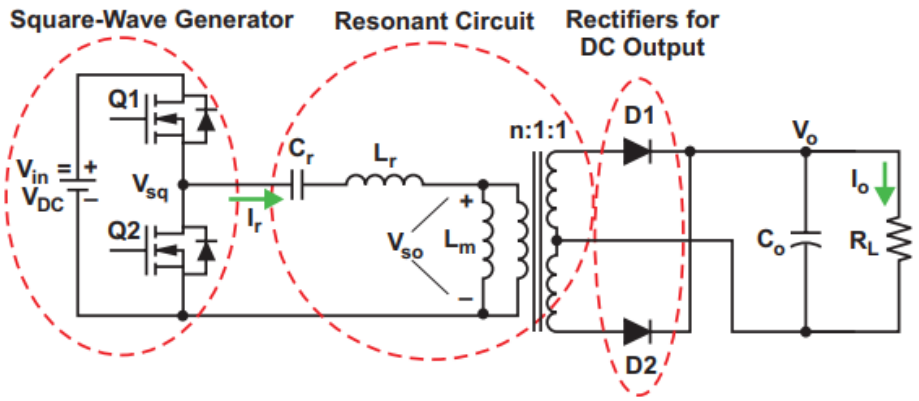

(a)

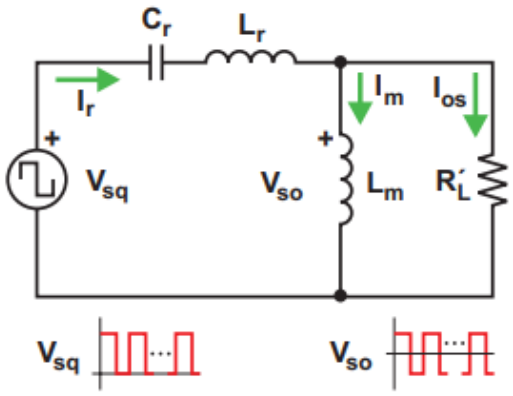

(b)

Fig. 2.2 Half-Bridge LLC Resonant converter. (a) Configuration. (b) Simpler Converter circuit.

2.4 Resonant Frequencies in a Square Wave Resonant Converter (SRC)

In essence, regardless of the frequency of the square-wave voltage provided at the input, the resonant network of a Square-Wave Resonant Converter (SRC) exhibits a minimal resistance to sinusoidal current at the resonant frequency. The selected attribute of the resonant circuit is the name given to this characteristic. The circuit's impedance steadily increases as resonance frequency decreases. The extent of current or energy that moves around and is distributed to the load is mostly determined by the magnitude of the impedance of the resonant circuit at the resonance frequency in conjunction with the load impedance. The energy given to the load is successfully managed by changing the resonant circuit's impedance via frequency modulation of the square-wave generator. This mechanism heavily relies on the series resonant frequency, which represents the system's sole resonance.

$$f_o = \frac{1}{2\pi\sqrt{L_r C_r}} \qquad (2.1)$$

The frequency of the circuit's highest resonance, fc0, is always equal to f0. So, an SRC needs a significant frequency variation to take input and output variations into account.

2.5 f_{c0}, f_0, and f_p in an LLC Circuit

The LLC circuit does, however, have unique features. The frequency at which the LLC circuit reaches peak resonance *(f_{c0})* changes depending on the load, ranging from f_p to f_{c0} to *f0,* with the addition of the second inductance (L_m). The pole frequency is still represented by equation (2.1), yet it is determined by a different parameter.

$$f_p = \frac{1}{2\pi\sqrt{(L_r + L_m)C_r}} \qquad (2.1)$$

When there is no load, the series resonant frequency (f_0) is equivalent to the pole frequency (f_p). However, as the load intensifies, the peak resonant frequency (f_{c0}) shifts closer to f_0. In the event of a short load, f_{c0} matches f_0. In contrast to the single curve that specifies $f_{c0} = f_0$ in the case of an (SRC), adjusting the impedance in an LLC resonant converter involves following a family of curves within the range of *fp* to f_{c0} to f_0. An LLC resonant converter can have a smaller frequency range needed because of this property, although circuit analysis is made more difficult.

Figure 2.3(b) shows unequivocally that whereas Equation (2.2)'s f_p only holds in the absence of a load, Equation (2.1)'s f_0 holds regardless of the load. Next, it will be shown that an LLC converter is usually designed to operate near to f_0. The functioning and design of the converter depend on f_0 for a variety of reasons, some of which are not made explicit.

2.6 Operation At, Below, and Above f_0

An LLC resonant converter's functionality is revealed by the connection between the (f_{sw}) and the (f_0). It is crucial to remember that the magnetizing current only flows on the primary side and does not give to the power delivery from the main-side source to the secondary-side load. The main-side current is produced by combining the magnetizing current with the secondary-side current, also referred to as the primary current.

2.7 At Resonance

The switching frequency and the series resonant frequency are synchronized in this operating mode. When switch *Q1* is turned off, power is no longer transmitted to the secondary side as the resonant current falls to the same level as the magnetizing current. Through the deliberate delay in activating switch *Q2*, the circuit achieves Zero Voltage Switching (ZVS) on the primary side, ensuring that the rectifier diodes on the secondary side undergo smooth and efficient commutation.

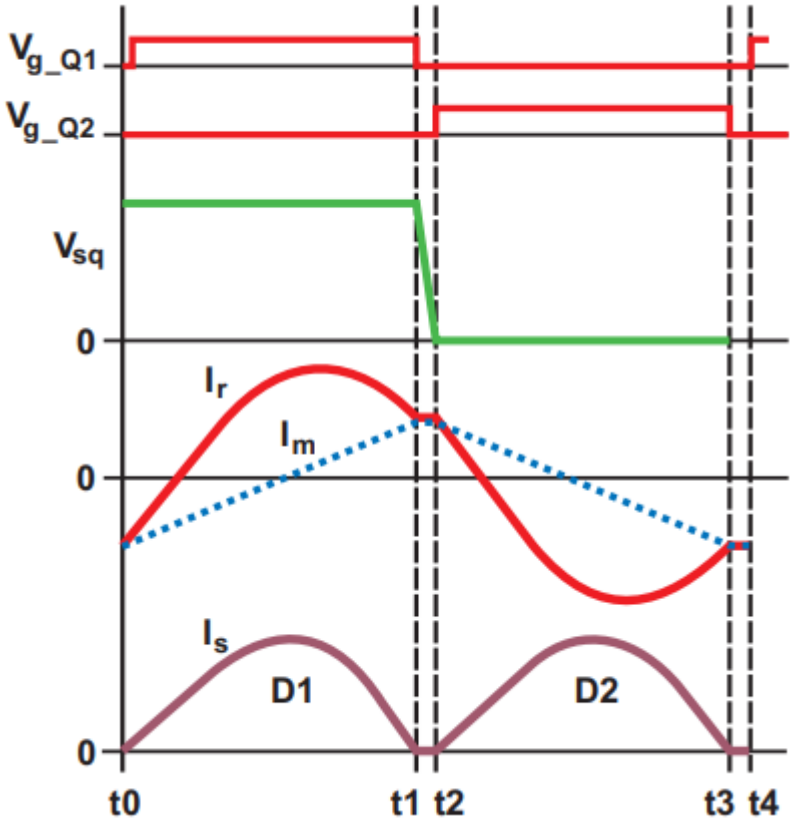

Fig. 2.3 At the Resonance frequency

2.8 Below Resonance

Even though the magnetizing current is still there in this case, power transmission stops because the resonant current equals the magnetizing current before the driving pulse width is finished. While still accomplishing primary Zero Voltage Switching (ZVS) and

permitting secondary soft commutation of the rectifier diodes, it is feasible to run below the series resonant frequency. The secondary-side diodes must work in discontinuous current mode, increasing the current that flows in the resonant circuit, to retain the same energy delivery to the load. Greater conduction losses develop on the main and secondary sides as a result of the enhanced current.

In addition, it is vital to keep in mind that basic ZVS may be affected if the f_{sw} goes too low. Massive switching losses and other problems may occur from this.

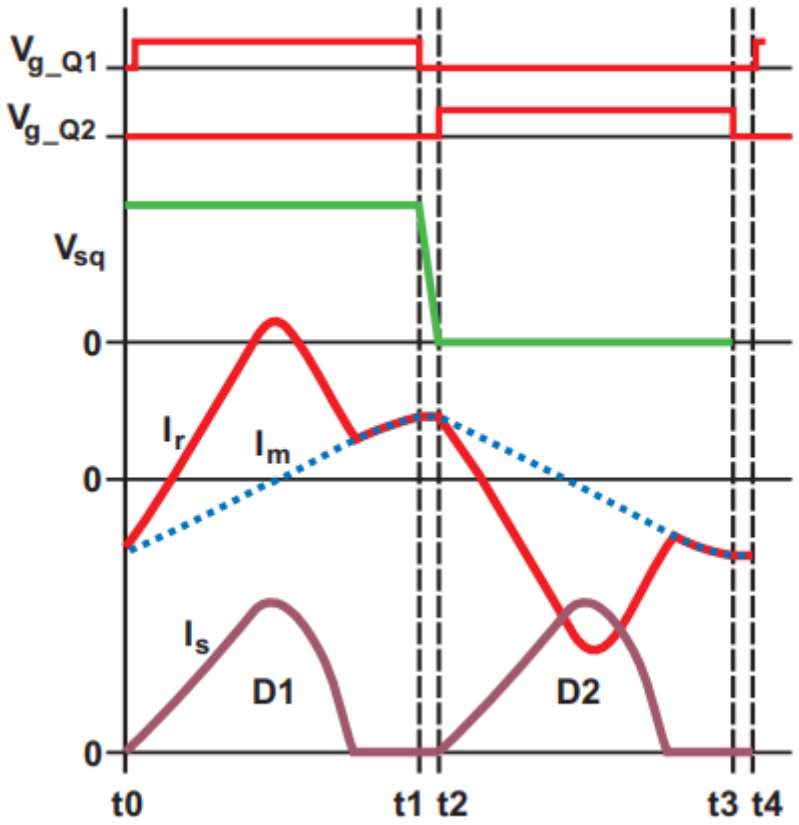

Fig. 2.4 Below Resonance frequency

2.9 Above Resonance

The primary side of the resonant circuit exhibits a reduced circulating current. This is due to the continuous-current mode of the resonant circuit's current, which leads to a lower RMS current for the same load, resulting in decreased conduction losses. Although there may be reverse recovery losses and the rectifier diodes are not softly

commutated, it is still feasible to attain primary Zero Voltage Switching (ZVS) when operating above the resonance frequency.

In light-load conditions, operating above the resonance frequency can lead to significant increases in frequency. The analysis that has come before has demonstrated that the converter may be created by altering f_{sw} on either side of f_0, using $f_{sw} = f_0$ or $f_{sw} > f_0$, or both.

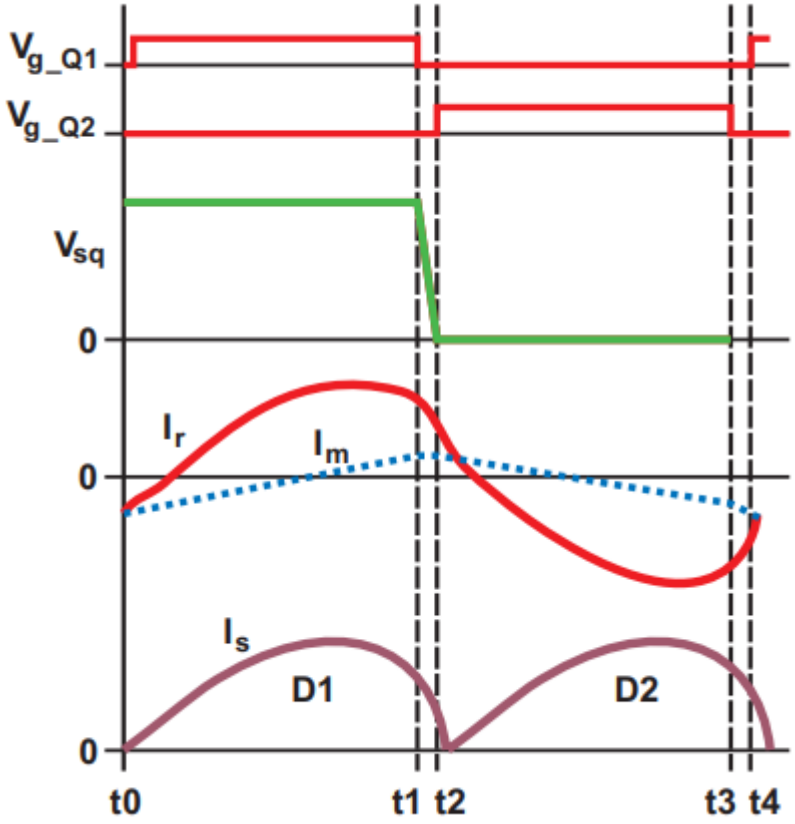

Fig. 2.5 Above Resonance frequency

Chapter 3

MODIFIED LLC RESONANT CONVERTER

Fig. 3.1 shows the construction of the I.S.O.P. Modified LLC resonant converter. As seen in Fig. 3.2, each section consists of two clamping diodes and a multi-transformer LLC converter. The output voltage of an ISOP (Input-Series-Parallel-Output) system is called *Vo*, while V_{in} is its total input voltage. Two split capacitors C_1 and C_2, two clamping diodes D_1 and D_2, and the resonant inductor L_r combine to form the resonant tank, as seen in Fig. 3.2. Lm is the isolated transformer's *n*-turns-per-inch magnetizing inductor.

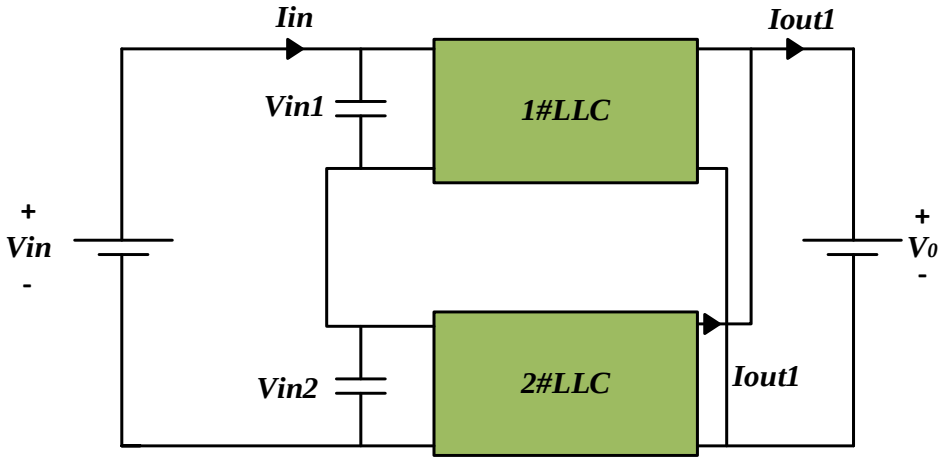

Fig. 3.1. Modular structure of the LLC converter.

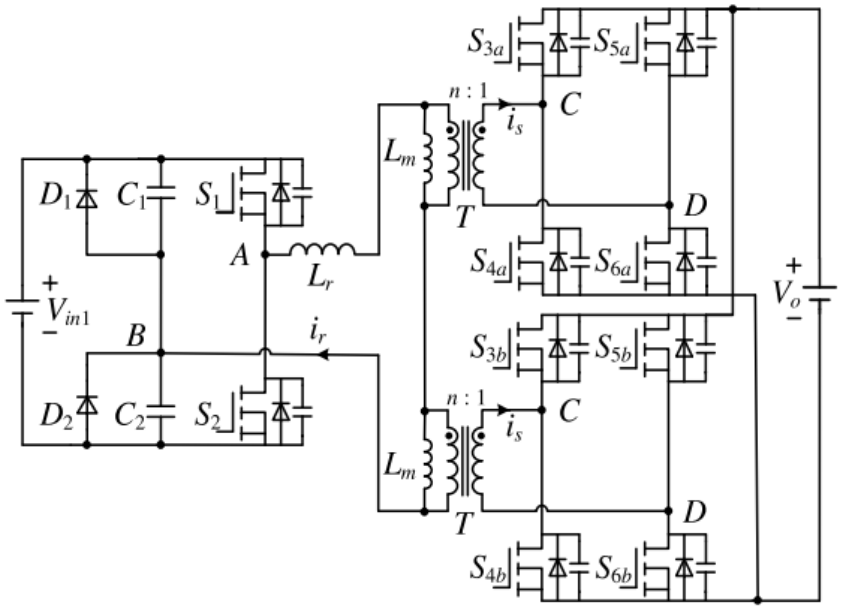

Fig. 3.2. Individual module

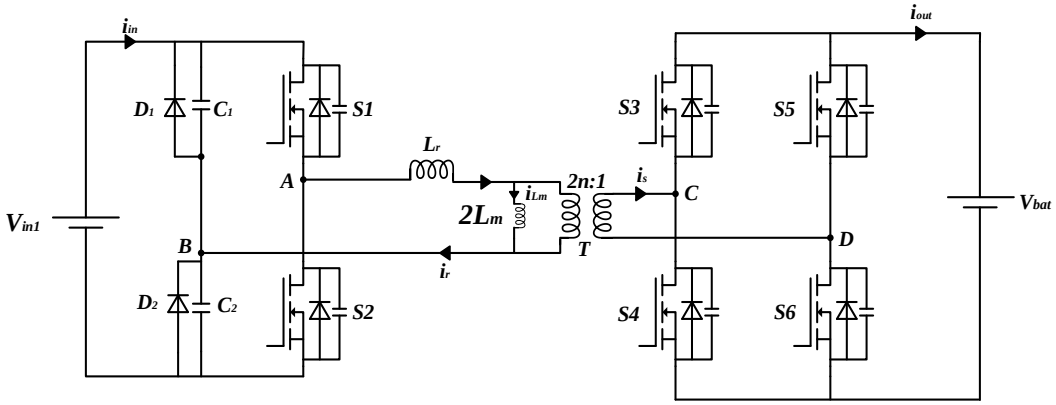

Fig. 3.3. Equivalent Bidirectional LLC resonant converter.

The resonant tank f_r frequency is indicated as follows:

$$f_r = \frac{1}{2\pi\sqrt{L_r(C_1 + C_2)}} \qquad (3.1)$$

The suggested system has two operational modes. When the EV battery is being charged and discharged using the correspondingly described Load Modes 1 and 2.

3.1 Mode 1: Forward Power Flow Operation

In this mode, power is transferred from the primary winding of the transformer to the secondary winding. Fig. 3.5 depicts the operating processes of this mode, while Fig. 3.4 depicts the primary waveform of the converter throughout this mode.

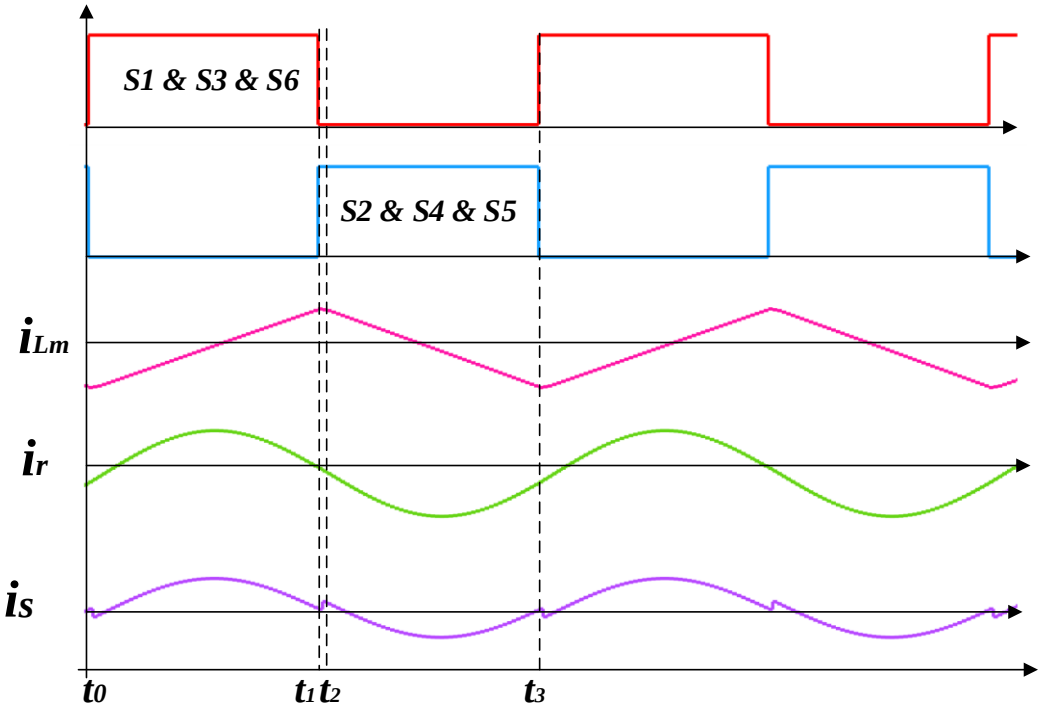

Fig. 3.4. Prime waveform during the forward power flow mode.

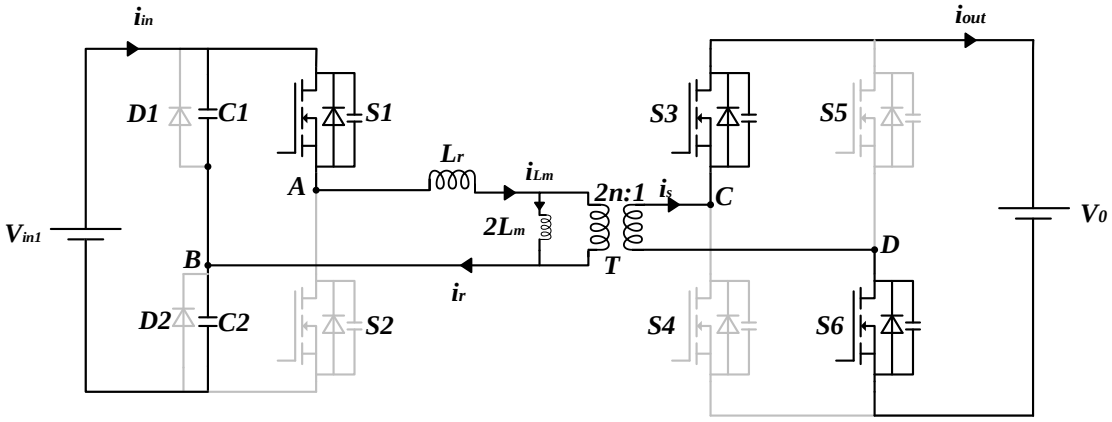

(a)

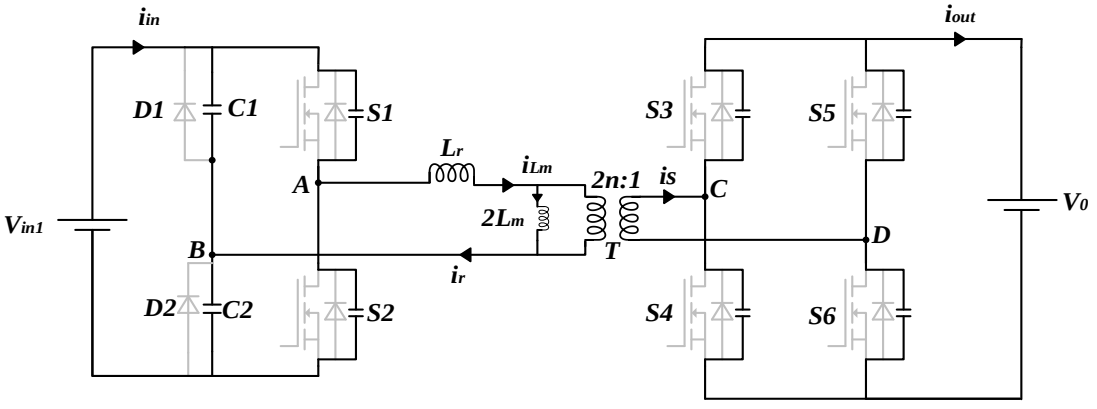

(b)

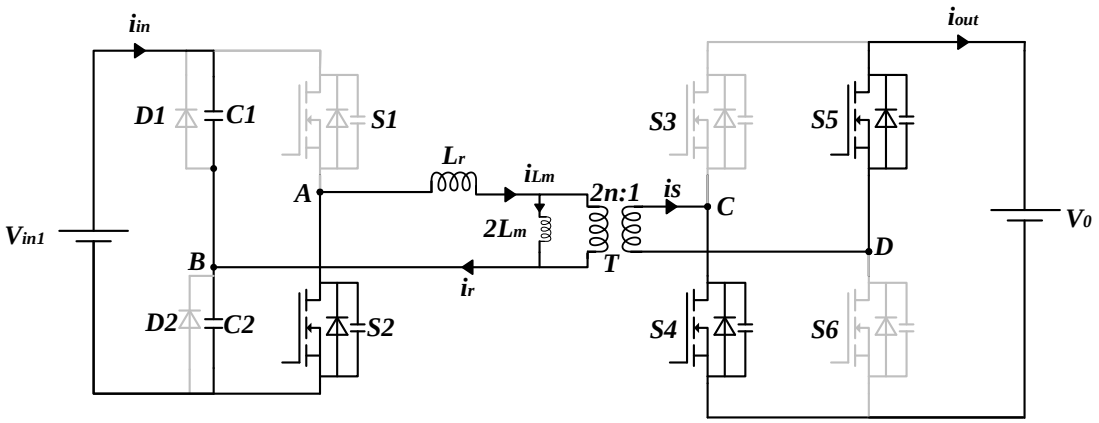

(c)

Fig. 3.5. Functioning of the converter in forward power flow mode. (a) Interval I. (b) Interval II. (c) Interval III.

Interval (I) [t_0–t_1; Fig. 3.5(a)]: S_1 and S_2 are turned off prior to t_0. Furthermore, junction capacitor voltages of S_3 and S_6 are reduced from V_0 to 0. S_3 and S_6's parasitic anti-parallel diodes then conduct, resulting in a ZVS state for S_3 and S_6. S_1, S_3, and S_6 are activated during this mode, and resonance occurs between C_1, C_2, and L_r. The effect of magnetizing current i_{Lm} on the voltage across L_m is that it becomes equal to nV_0. Initially, it decreases in the negative direction followed by an increase in the positive direction which results in the i_s of the transformer equal to $2n(i_r$-$i_{Lm})$.

Interval (II) [t_1–t_2; Fig. 3.5(b)]: S_1, S_3, and S_6 are turned off at $t = t_1$ and the resonant current becomes equal to zero. The junction capacitor of switch S_1 and S_2 resonate the L_r. After that, the i_{Lm} is decreasing in a positive direction which makes the voltage of L_m inversed.

Interval (III) [t_2–t_3; Fig. 3.5(c)]: At this stage, S_2, S_4, and S_5 are turned on, and the i_r starts increasing in a positive direction like in Interval (I).

Mode 2: Reverse Power Flow Operation

The battery is being discharged while it is operating in this mode.

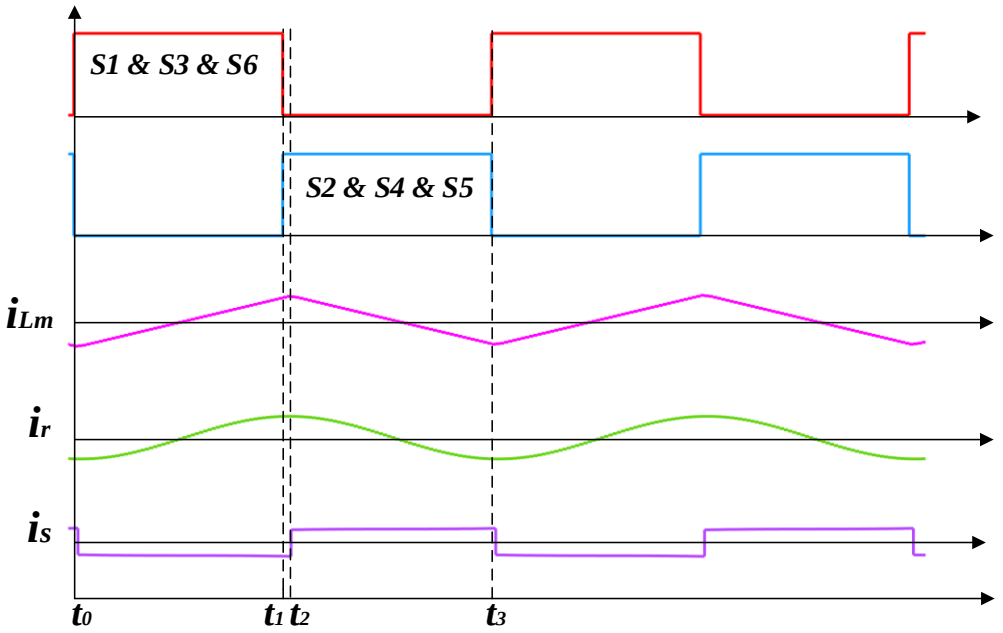

Fig. 3.6. Prime waveforms during Reverse power flow mode.

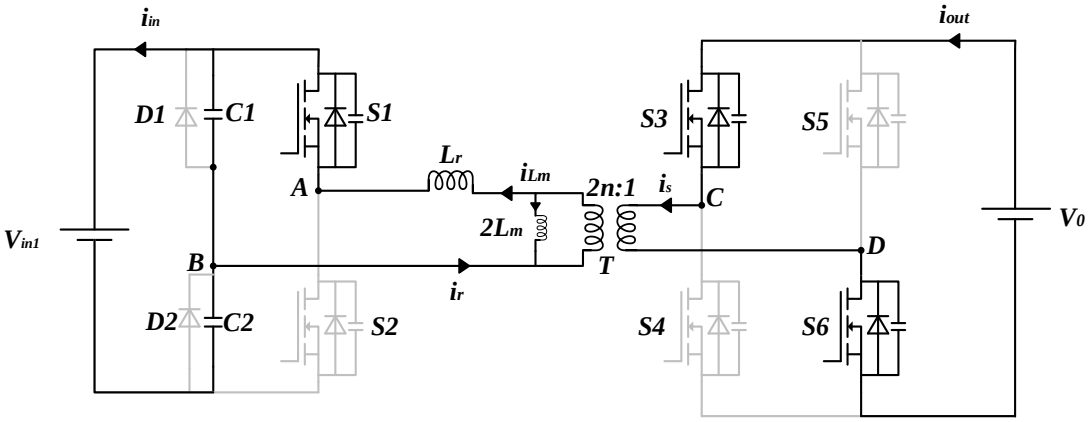

(a)

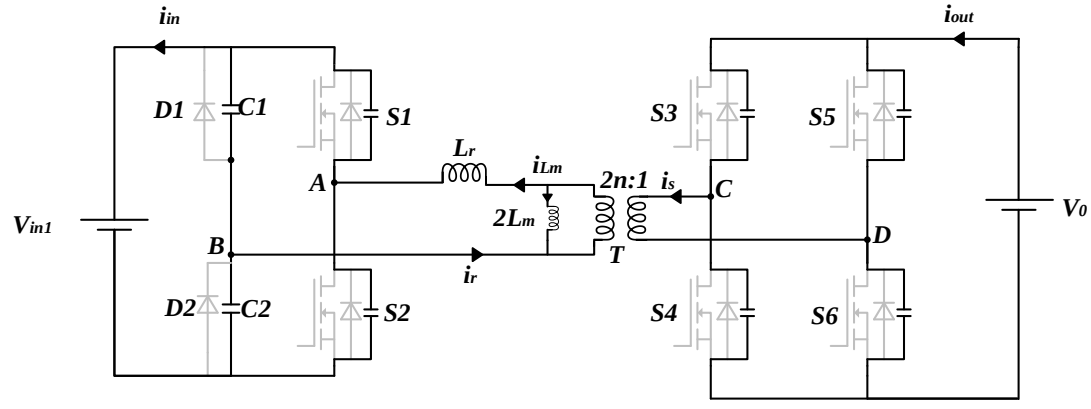

(b)

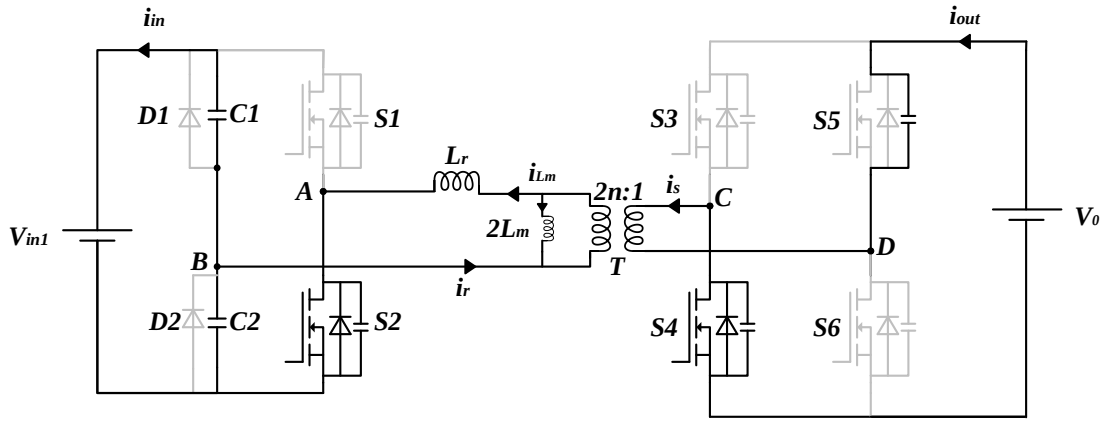

(c)

Fig. 3.7. Functioning of the converter in reverse power flow mode. (a) Interval I. (b) Interval II. (c) Interval III.

Interval (I) [t_0–t_1; Fig. 3.7(a)]: S_1, S_3, and S_6 are off before this mode. Additionally, the voltage across S_1's junction capacitor has reduced to zero, creating the necessary conditions for S_1 to achieve ZVS, conducting the anti-parallel diode of S_1. S_1, S_3, and S_6 are turned on at time $t = t_0$, and resonance between C_1, C_2, and L_r takes place. As it moves away from zero, the i_{Lm} reduces negatively in a linear manner. After changing to zero, the i_{Lm} will start to rise in a positive direction. When the secondary current i_s reduced to zero, this mode ends.

Interval (II) [t_1–t_2; Fig. 3.7(b)]: S_1, S_3, and S_6 are turned off at $t = t_1$. When the junction capacitor voltage of S_2 drops to zero, L_r resonates with the junction capacitor of S_3, S_4, and S_5. After that, an anti-parallel diode is conducted. The i_{Lm} is then reduced in the positive direction in a linear manner once the voltage across L_m is reversed.

Interval (III) [t_2–t_3; Fig. 3.7(c)]: The conductivity of S_2's anti-parallel diode assures that S2's ZVS will switch on before time $t = t_2$. S_2, S_4, and S_5 are on at $t=t_2$ which is similar to the interval (I).

Chapter 4

ZVS ANALYSIS FOR CONVERETR

4.1 Zero Voltage Switching

To achieve Zero Voltage Switching (ZVS), it is essential to ensure that the junction capacitors are fully charged or discharged using the energy stored in the resonant inductor before activating the switches. As illustrated in Fig 4.1, when switches S_1, S_3, and S_6 are turned off, the current flowing through the resonant inductor decreases to zero and reaches a value of i_{Lm}. This discharge of current helps in charging or discharging the junction capacitors associated with switches S_4 and S_5. Subsequently, the antiparallel diodes of S_4 and S_5 conduct until S_4 and S_5 are turned on. To ensure that switches S_4 and S_5 achieve the ZVS state when turned on, it is necessary to appropriately design the magnetizing current of the transformer. The magnetizing current of the transformer should possess enough energy to effectively charge or discharge the junction capacitors. It is necessary for the energy stored in the magnetizing inductor to exceed the energy stored in the four junction capacitors to ensure complete charging or discharging of the junction capacitors.

$$\frac{1}{2} L_m i_{Lm\_peak}^2 \geq \frac{1}{2} (C_{S3} + C_{S4} + C_{S5} + C_{S6}) V_0^2. \qquad (4.1)$$

where C_{S3}, C_{S4}, C_{S5}, and C_{S6} are the junction capacitor of respective of the respective switch.

$$i_{Lm\_peak} = \frac{nV_0}{4L_m f_s}. \qquad (4.2)$$

During the dead time, the magnetizing inductor's current should be greater than zero.

$$i_{Lm\_peak} - T_{dead} \frac{nV_0}{L_m} \geq 0. \qquad (4.3)$$

where T_{dead} is dead time and is described below:

$$T_{dead} = \frac{1}{2 f_s} - \frac{1}{2 f_r}. \qquad (4.4)$$

According to (4.2) and (4.3), the magnetizing inductance range may be determined and stated as follows:

$$L_m \le \frac{n^2}{64 f_s C_{S3}}. \qquad (4.5)$$

It can be concluded from (4.4) and (4.5) that

$$2 f_s \ge f_r. \qquad (4.6)$$

$$\frac{1}{2} L_r i_{Lm\_peak}^2 \ge \frac{1}{2} (C_{S1} + C_{S2}) V_{in1}^2. \qquad (4.7)$$

It is anticipated that C_{S1} and C_{S2} have the same value. According to (4.2) and (4.7), the magnetizing inductance range is,

$$L_m \le \sqrt{\frac{n^2 V_0^2 L_r}{32 C_{S1} f_s V_{in1}}}. \qquad (4.8)$$

The range of the magnetizing inductance is illustrated in the above analysis as (4.7) and (4.8). According to (4.6), to satisfy ZVS the twice of switching frequency must be greater than the resonating frequency.

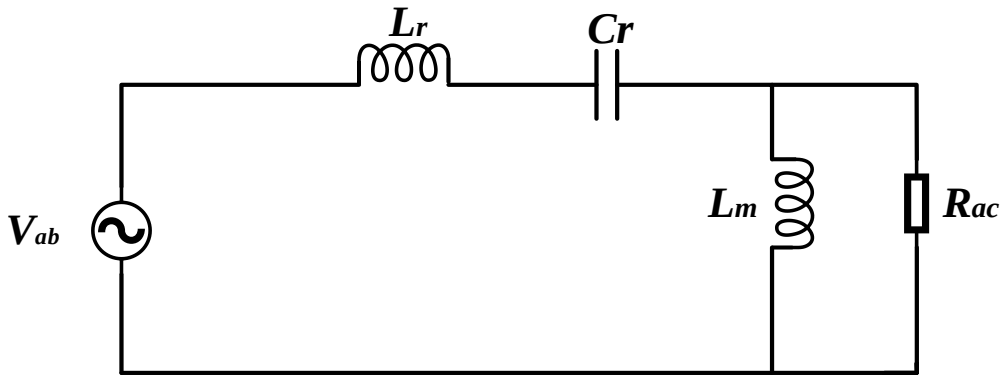

Fig. 4.1. Equivalent model of the LLC converter.

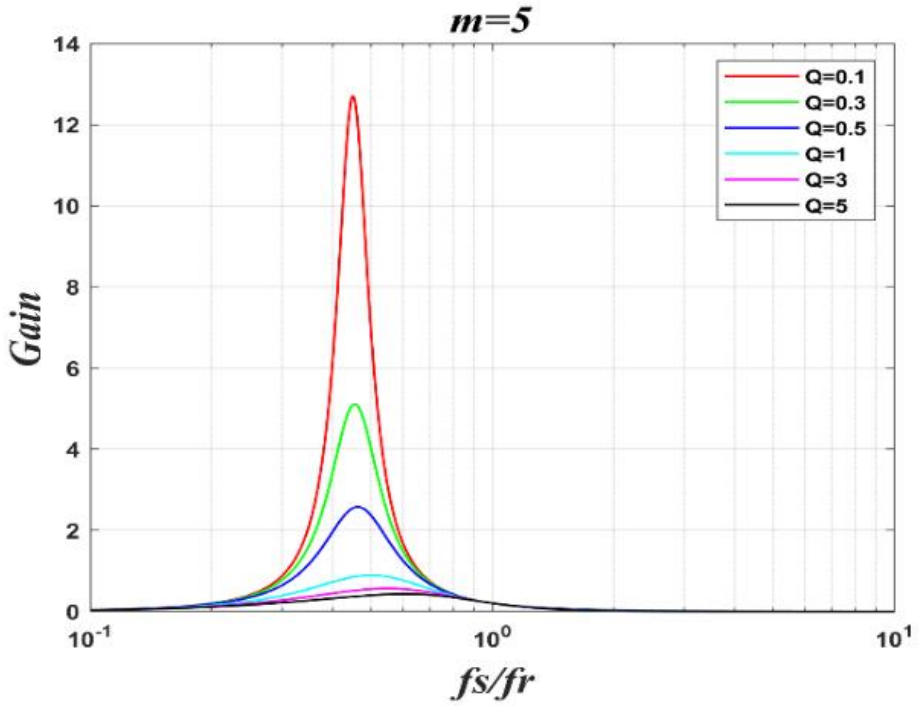

Fig. 4.2. Gain characteristics under variable frequency.

$$R_{ac} = \frac{8n^2 R_0}{\pi^2}. \tag{4.9}$$

R_0 is the actual load of the converter and f_r is the resonating frequency.

$$f_r = \frac{1}{2\pi\sqrt{L_r C_r}}. \tag{4.10}$$

LLC converter Gain is described below:

$$M = \frac{\{f^2.(m-1)\}}{\sqrt{\{(m.f^2-1)^2 + f^2(f^2-1)^2.(m-1)^2.Q^2\}}}. \tag{4.11}$$

where

$$f = \frac{f_s}{f_r}. \tag{4.12}$$

$$Q = \frac{\sqrt{L_r / C_r}}{R_{ac}}. \tag{4.13}$$

$$m = \frac{L_r + L_m}{L_r}. \tag{4.14}$$

$$f_r = \frac{1}{2\pi\sqrt{L_r C_r}}. \quad (4.15)$$

4.2 DESIGN CONSIDERATION

4.2.1. Transformer turns ratio

The transformer turns ratio for this converter is described as:

$$n = \frac{V_{in}}{8V_0}. \quad (4.16)$$

4.2.2. Design of Resonant Tank

$$C_1 = \frac{P_{\max}}{2 f_s V_{in1}^2}. \quad (4.17)$$

where P_{max} denotes each LLC converter's maximum output power. Furthermore, the resonant inductance may be determined using,

$$Lr = \frac{1}{8\pi^2 C_1 f_s^2}. \quad (4.18)$$

4.2.3. Current Stress of the Clamping Diodes

When the voltage across C_1 falls to zero, D_1 begins to conduct. The current in D_1 then reduces linearly when the voltage across L_r reduced to $-2nV_o$. When S_1 turns off the voltage across L_r changes to $-(2nV_o + V_{in1})$. As a result, the current of D_1 may be represented as follows:

$$i_{D1}(t) = \begin{cases} i_{D1\_1} = I_{D\max} - \dfrac{2nV_0}{L_r}(t - t_1), t_1 < t \le t_2 \\ i_{D1\_2} = i_{D1}(t_2) - \dfrac{V_{in} + 2nV_0}{L_r}(t - t_2), t_2 < t \le t_3 \end{cases}. \quad (4.19)$$

where I_{Dmax} is the current of D_1 at $t = t_1$, as illustrated:

$$I_{D\max} = i_r(\Delta t) \quad (4.20)$$

In addition, t_2 can be solved by

$$t_2 - t_1 = \frac{1}{2 f_s} - \Delta t. \quad (4.21)$$

Because the current of D_1 goes to zero at $t = t_3$, t_3 may be computed as:

$$t_3 = \frac{V_{in} + 2 f_s L_r I_{D\max} + 4 t_1 f_s V_0 n}{2 f_s V_{in} + 4 f_s V_0 n}. \qquad (4.22)$$

The rms of $i_{D2}(t)$ may thus be stated as (23):

$$i_{D1\_RMS} = \sqrt{2 f_s (\int_{t_1}^{t_2} i_{D1\_1}^2 dt + \int_{t_2}^{t_3} i_{D1\_2}^2 dt}. \qquad (4.23)$$

4.3 Observed Waveforms of Modified LLC Converter for ZVS

(a)

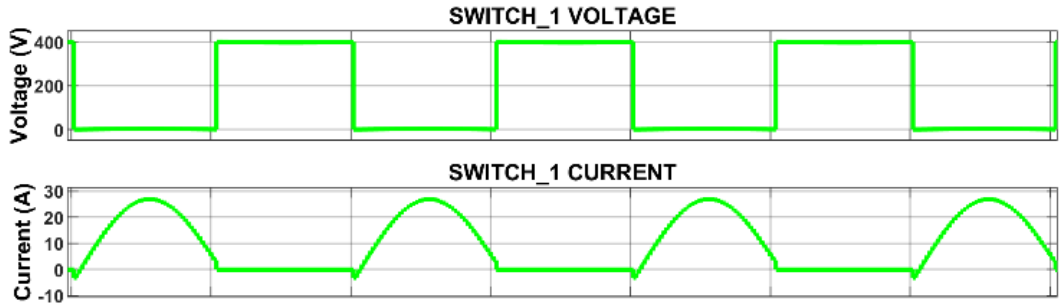

(b)

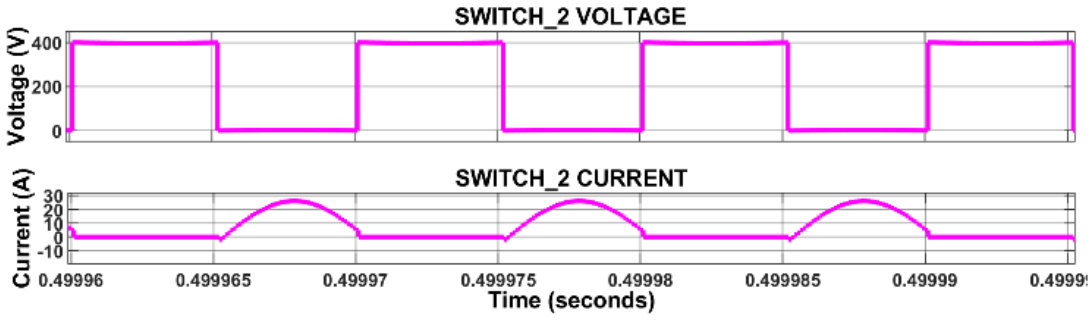

(c)

Fig. 4.3. Resonating nature of switches during charging. (a) Pulses. (b) voltage & current waveform for switch 1. (c) voltage & current waveform for switch 2.

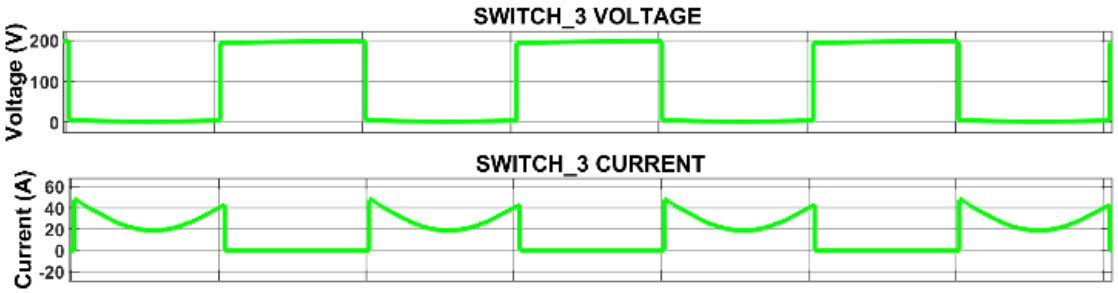

(a)

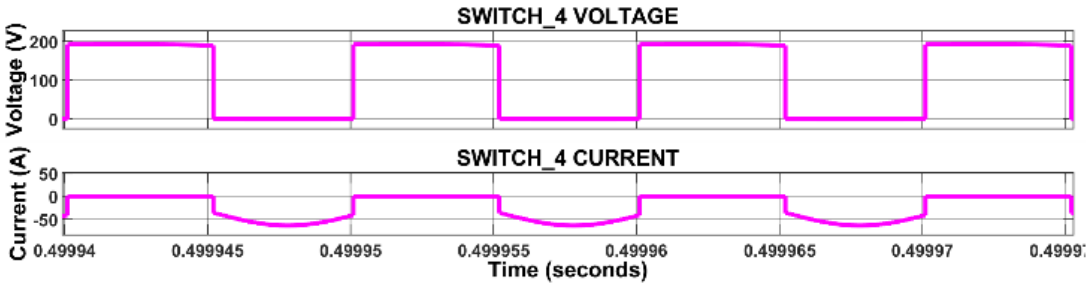

(b)

Fig. 4.4. Resonating nature of switches during charging. (a) voltage & current waveform for switch 3. (b) voltage & current waveform for switch 4.

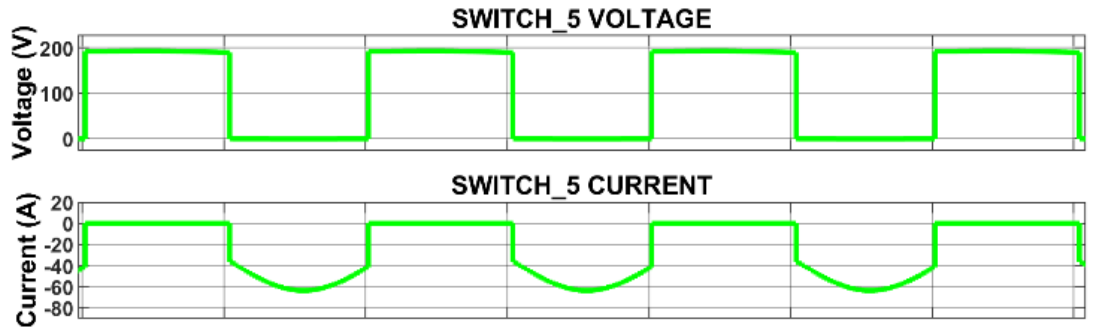

(a)

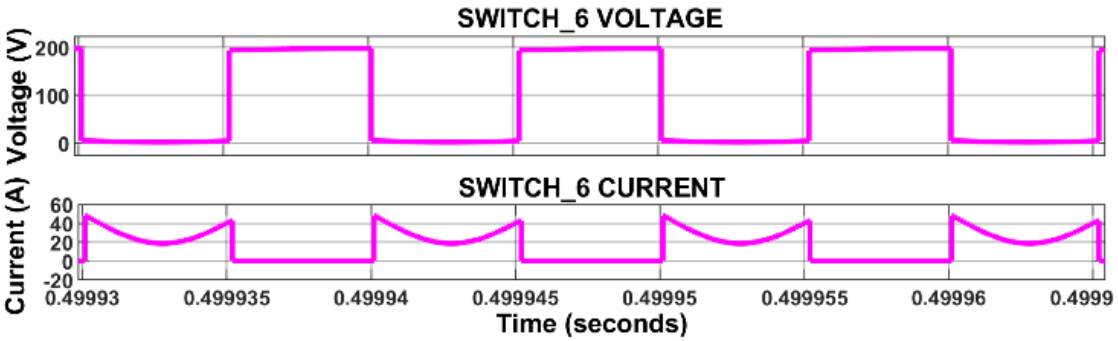

(b)

Fig. 4.5. Resonating nature of switches during charging. (a) voltage & current waveform for switch 5. (b) voltage & current waveform for switch 6.

The resonating nature of the LLC converter in forward mode is seen in the above figures. The waveforms are enlarged to demonstrate ZVS's appropriate behaviour. In the proposed system, all MOSFET switches have the appropriate junction capacitor to ensure the ZVS condition, which explains why the system's efficiency is excellent at any load.

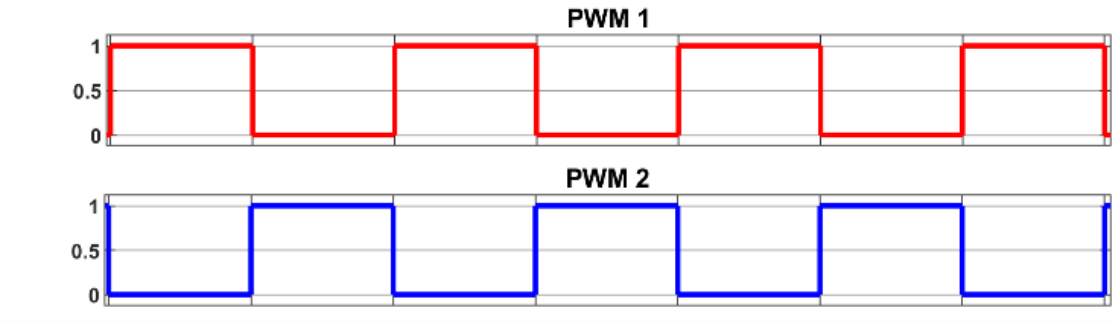

(a)

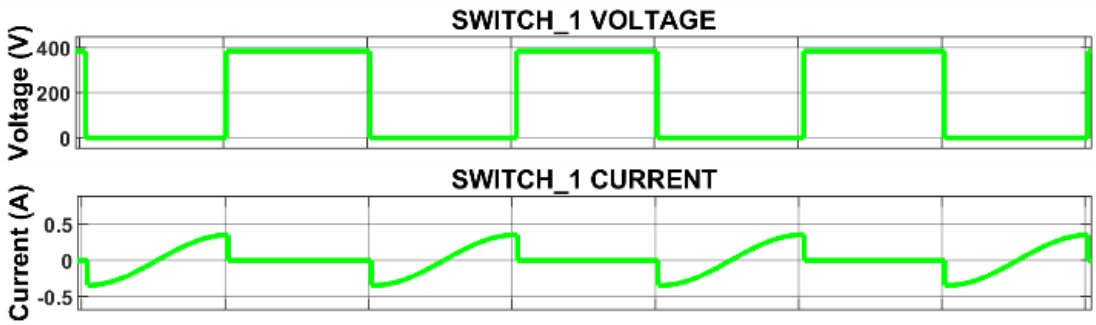

(b)

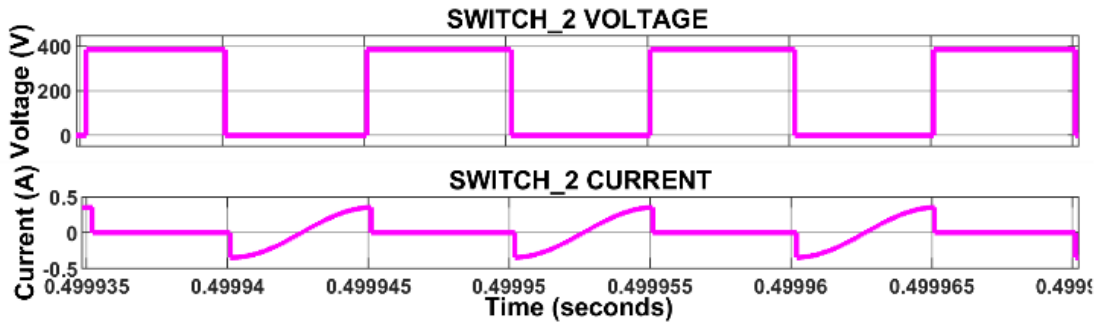

(c)

Fig. 4.6. Resonating nature of switches during discharging. (a) Pulses. (b) voltage & current waveform for switch 1. (c) voltage & current waveform for switch 2.

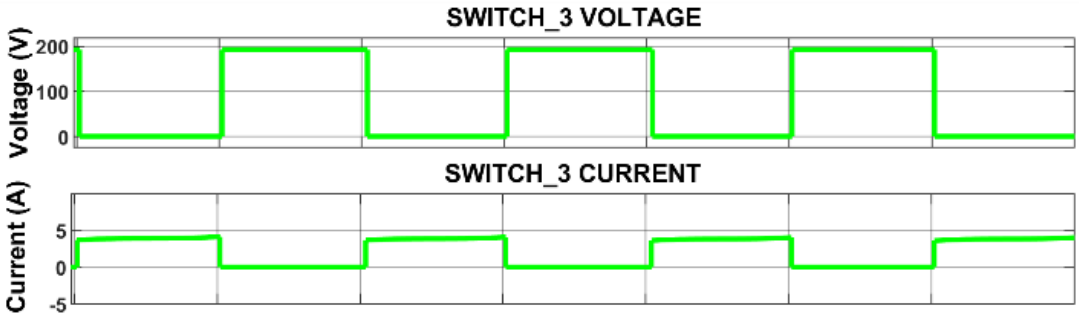

(a)

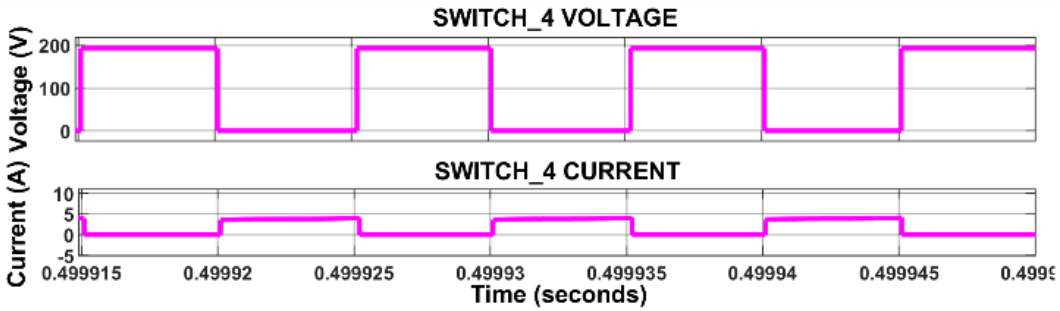

(a)

Fig. 4.7. Resonating nature of switches during discharging. (a) voltage & current waveform for switch 3. (b) voltage & current waveform for switch 4.

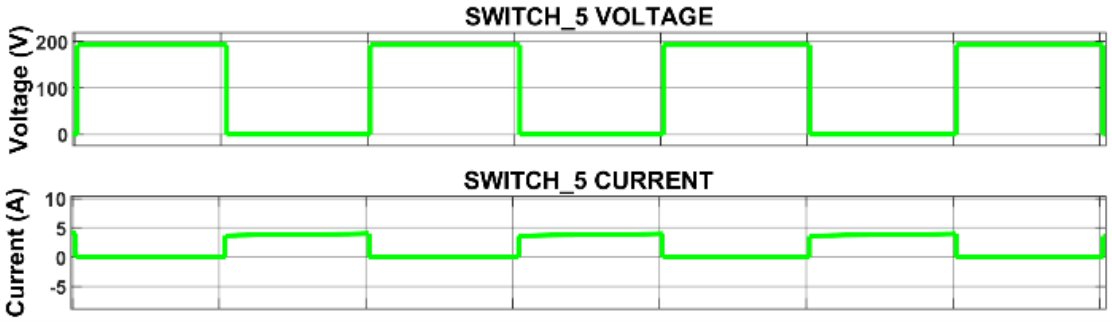

(a)

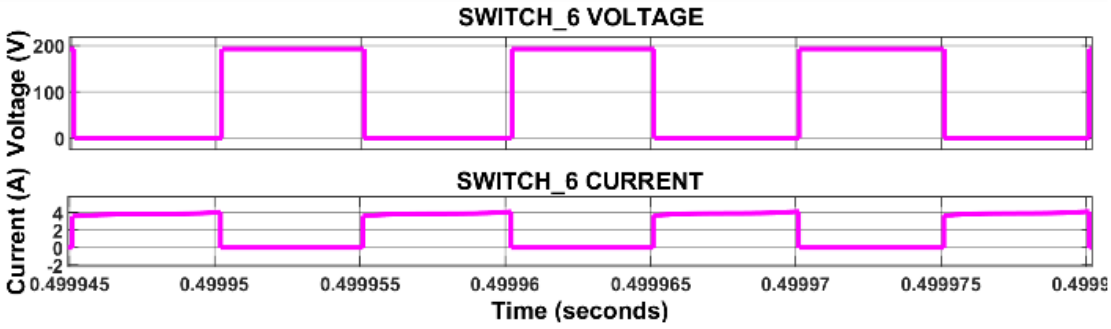

(b)

Fig. 4.8. Resonating nature of switches during discharging. (a) voltage & current waveform for switch 5. (b) voltage & current waveform for switch 6.

The resonating nature of the power converter in reverse mode is seen in the above figures. In this mode of operation, the converter maintains ZVS at all times in each MOSFET switch, which explains why the efficiency remains quite high when discharging.

Chapter 5

SYSTEM CONFIGURATION

5.1 Overview

The architecture utilized for EV chargers is depicted in Fig. 5.1. The system consists of two conversion stages, the initial of which is an AC-DC conversion stage and the other of which is a DC-DC conversion stage. With the suggested controlled arrangement, the first stage AC-DC converter functions as a regulated rectifier. The second stage is a modified LLC converter with six MOSFET switches with ZVS characteristics. The Lithium Ion battery is charged after the second stage with Constant Current (CC) charging.

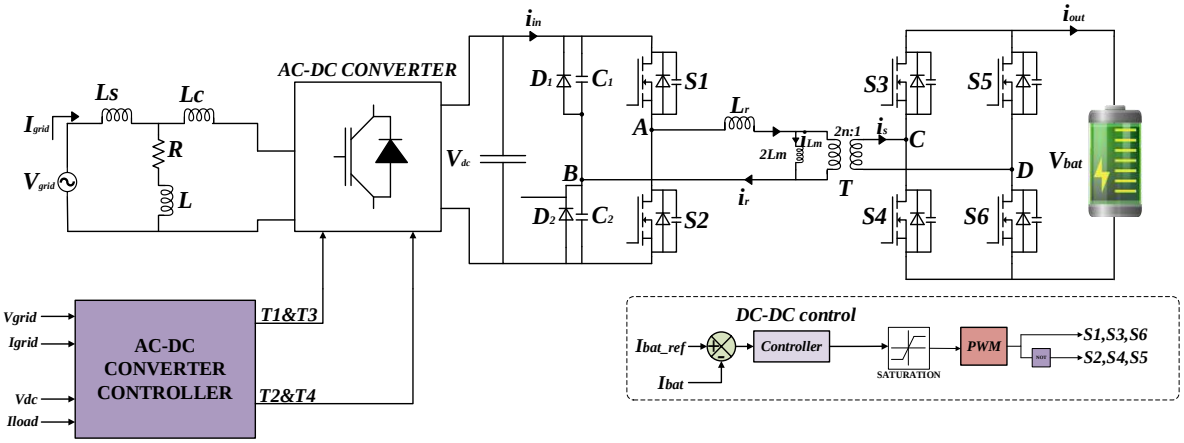

Fig. 5.1. Circuit Diagram of System Configuration for On-Board EV charger (G2V operation).

5.2 SECOND-ORDER GENERALIZED INTEGRATOR METHOD: [SOGI]

The SOGI block's goal, as previously mentioned, is to provide two in-phase, in-quadratic signals to the mains voltage. The percentage of errors is *K* times increased whenever the supply is first compared to the in-phase signal. This parameter has a substantial impact on the overall efficacy of SOGI. This block adapts the system to shifting frequencies by using the ω ` created by the 2nd half of the configuration.

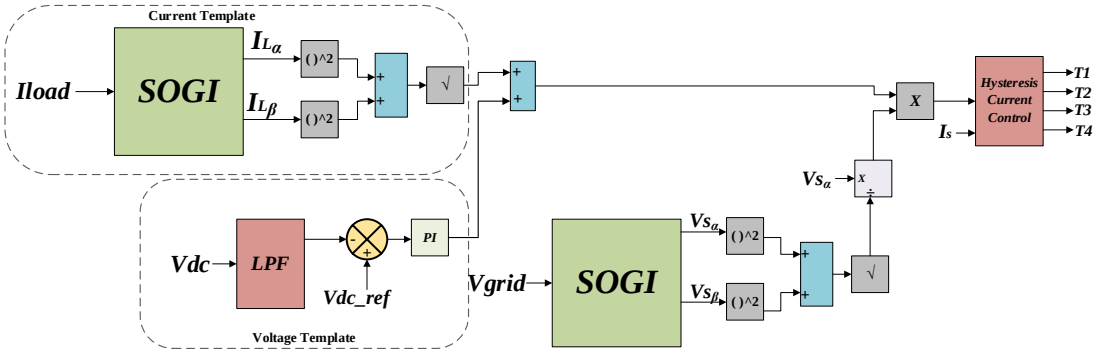

Fig. 5.2. Control scheme for AC-DC converter stage.

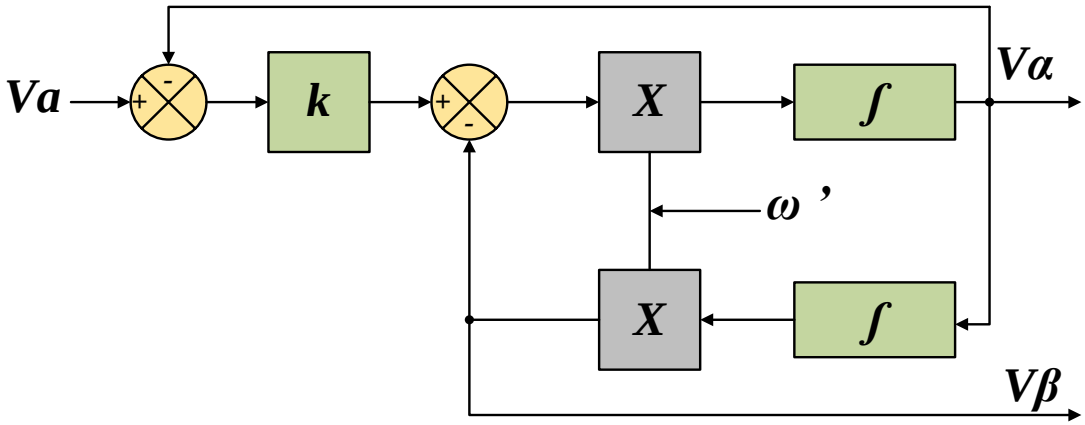

Fig. 5.3. Representation of SOGI controller.

The aforementioned block can eliminate the *100Hz* and *120Hz* frequency components from the detected sample. The frequency spectrum arrangement of SOGI is as outlined below:

$$SOGI = \frac{\omega s}{\omega^2 + s^2} \qquad (5.1)$$

ω is the resonance frequency, commonly referred to as the basic angular frequency. For voltages α and β, the closed-loop conversion function is presented in (5.2) and (5.3), below:

$$H_\alpha(s) = \frac{v_\alpha(s)}{v(s)} = \frac{k\omega s}{s^2 + k\omega s + \omega^2} \qquad (5.2)$$

$$H_\beta(s) = \frac{v_\beta(s)}{v(s)} = \frac{k\omega^2}{s^2 + k\omega s + \omega^2} \qquad (5.3)$$

$H_\alpha(s)$ is a 2nd-order BPF with no phase shift, while $H_\beta(s)$ is a 2nd-order low-frequency filter with gain equal to 1 and 90° phase departure at 314 *rad/s*.

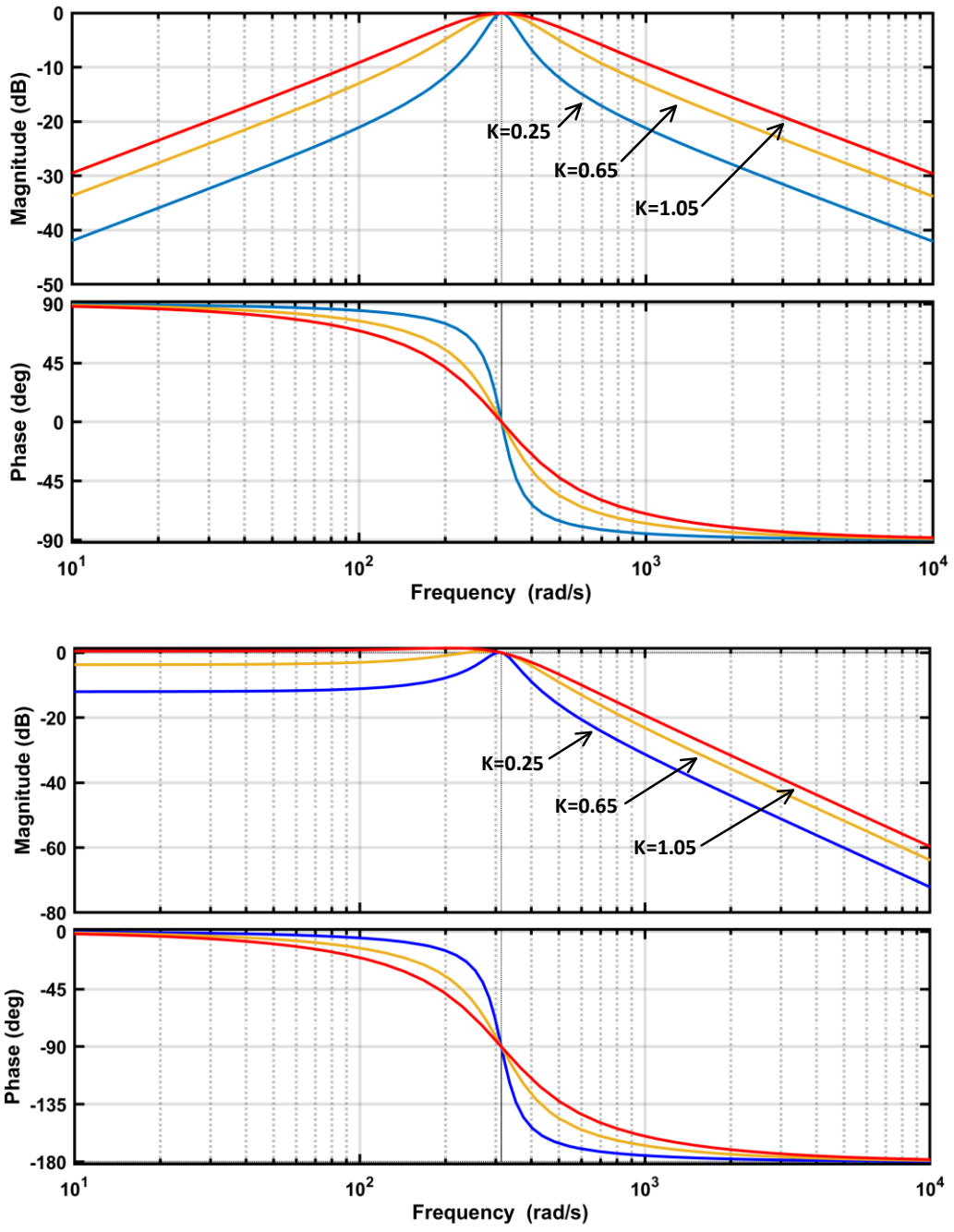

Fig. 5.4. Bode plot of SOGI filter (a). Hα(S) for different values of K. (b). Hβ(S) for different values of K.

By using a SOGI filter, the basic aspect of the load current is removed. The SOGI block processes the supplied signal (I_{load}), which results in the equal-phase and quadrature-phase signals I_α and I_β respectively, being produced at the output. Thus, it is possible to determine the basic current (I_f) using

$$I_f = \sqrt{I_f{}^2 + I_\beta{}^2} \qquad (5.4)$$

To determine the switching loss in the shunt compensator using the V_{dc_ref}*, the V_{dc} is traversed through an LPF. Using the inaccuracy of the dc link voltage as input, a PI controller computes the switching loss (I_{loss}) of the recommended system. A steady *400V* DC connection voltage is sustained. The formula is described below:

$$I_{loss}(k) = [(k_p + k_i / s)(V_{dc\_ref}{}^*(k) - V_{dc}(k))] \qquad (5.5)$$

where kp and ki are the PI controller's gain coefficients. Equation (4.5)'s DC link loss component and fundamental load current component are added to get the total reference current magnitude (I_{tot}).

$$I_{tot} = I_{loss} + I_f \qquad (5.6)$$

Now, the following equation is used to produce the unit template (u_a).

$$u_a = \frac{v_\alpha}{\sqrt{v_\alpha{}^2 + v_\beta{}^2}} \qquad (5.7)$$

Multiplying the total reference current by the unit template yields the reference current.

$$I_{ref} = I_{tot} * u_a \qquad (5.8)$$

Finally, gating pulses are produced for GSC's IGBT switches (insulated gate bipolar transistors) using a hysteresis current controller (HCC). In Fig. (5.2), the full control system is shown.

5.3 PI CONTROLLER FOR DC-DC CONVERTER

The battery current I_{bat} is controlled by the PI controller. During Forward power flow mode, the described controller is employed to maintain the necessary battery current. When the battery is discharged through a load in the reverse power flow mode, the desired battery current is maintained. The controller's output is compared to a sawtooth signal, and the comparison output is a PWM signal that operates the power converter switches. The PID controller's output (u(t)) depends on the system's error signal *(e(t)),* as explained.

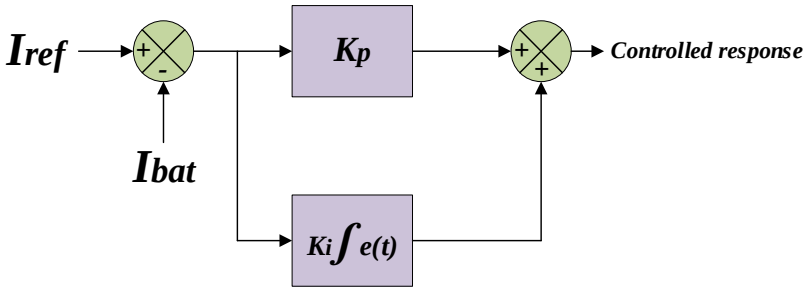

Fig. 4.5. PI controller for DC-DC converter stage.

$$u(t) = K_p.e(t) + K_I \int e(t)dt + K_D \frac{de(t)}{dt} \qquad (5.9)$$

PID gains can be adjusted using a variety of methods based on the mathematical model of the plant. The closed-loop system's transient and steady-state requirements determine the PI gains. The most well-known method for adjusting PI gains is the Ziegler and Nichols method, which proposes guidelines for adjusting PI controllers (i.e., setting values for K_p and T_i,) based on experimental step responses or the value of K, leading to marginal stability when only proportional control action is used.

Chapter 6

RESULTS: SIMULATION AND EXPERIMENTAL

6.1 Parameters Used in the Simulation

TABLE 6.1.

PARAMETERS	
Item	***Details***
Grid Voltage (V_g)	230V (*rms*)
DC Link Voltage (V_{in})	400V
Battery Voltage (V_{bat})	180V
Rated Power *(P)*	3.3kW
Turns Ratio (*n)*	1:4
Resonant Capacitance (C_1 & C_2)	0.1µF
Resonant Inductance (L_r)	12.3µH
Magnetizing Inductance (L_m)	420µH
Switching Frequency (f_s)	100kHz
Output Filter Capacitor (C_o)	44µF

6.2 Modified LLC converter as Bidirectional operation

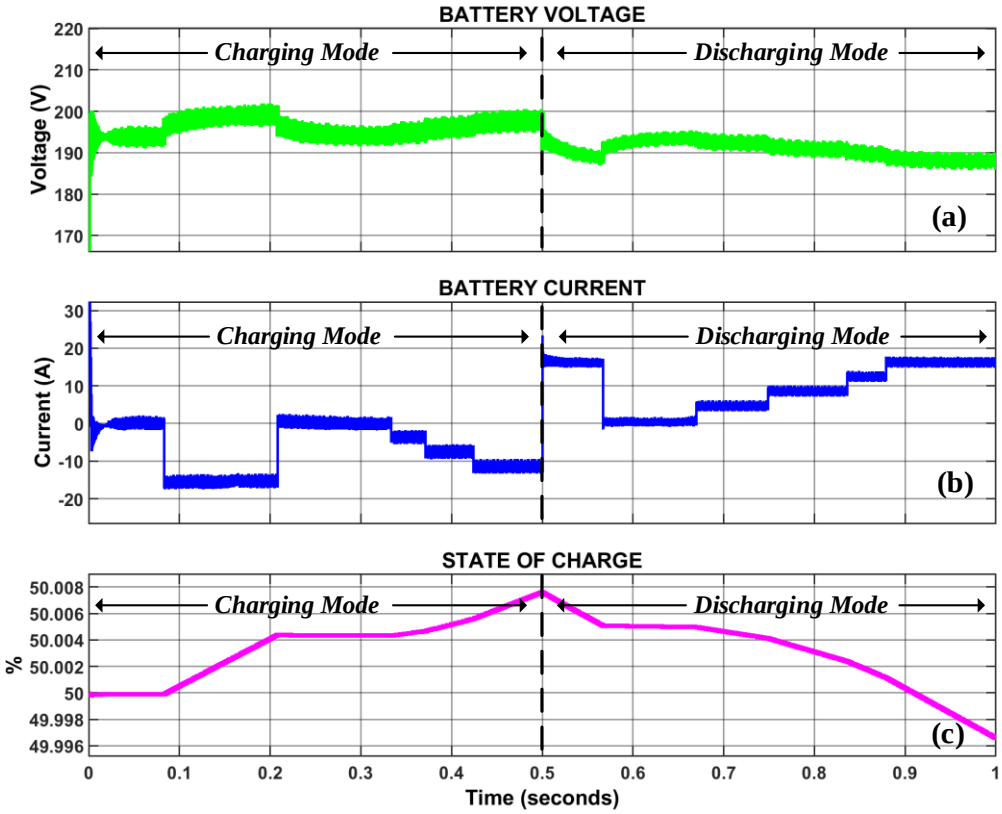

Fig. 6.1. Battery characteristics. (a) Battery voltage. (b) Battery current. (c) State of charge.

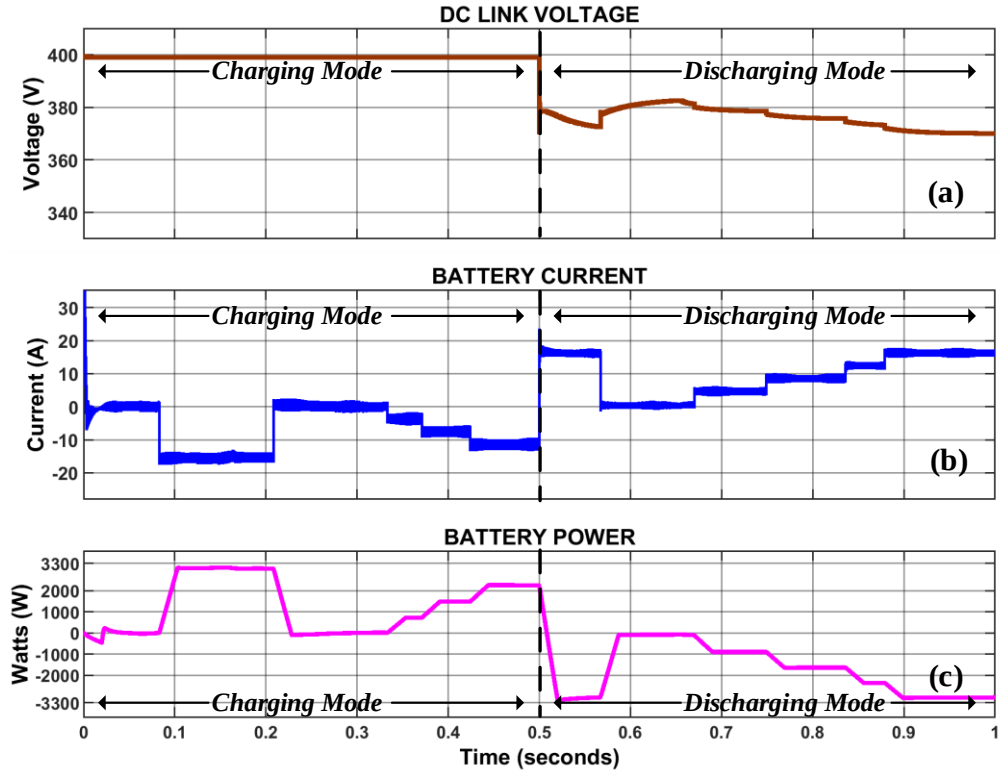

Fig. 6.2. (a) DC link voltage. (b) Battery current. (c) Battery Power.

The above graphs show the Battery charging mode and discharging mode of operations and their effects on the voltage, current, SOC (State of charge), and Power.

6.2.1 Charging Mode

All loads are connected at time *t=0s*, therefore the battery receives zero power; as a result, it exhibits constant characteristics as shown in Fig. 6.1 (c). At this point, the battery is not charging and is not consuming any power from the source. Parallel loads are disconnected at *t=0.08s*, causing SOC to increase quickly, current to increase in the opposite direction as shown in Fig. 6.1 (b), battery voltage to improve as shown in Fig. 6.1 (a), and power to be maintained up to rated limit. The same loads are connected once more at time *t=0.23 s*. At *t=0.33s*, loads are disconnected one at a time, making the charge slope steeper over time. Additionally, currents exhibit a rising character in the opposite direction. Power is changing according to the load transients as shown in Fig. 6.2 (c).

6.2.2 Discharging mode

At *t=0.5s* since all loads are connected in this mode, the battery is being discharged, resulting in positive current values and negative power readings because in this mode battery is acting as a source as described in Fig. 6.1 Since the battery is currently attempting to maintain the regulated DC Link Voltage as shown in Fig. 6.2 (a), which is also being impacted at this moment, due to converter's ability to operate in both directions. Since there are no loads connected at *t=0.56s*, the SOC curve is constant, and the dc link voltage increases since there is nothing for the battery to discharge. At *t=0.67s*, loads begin to increase one at a time, which speeds up battery discharge and causes voltages to drop.

6.3 G2V Operation of proposed system

By modeling under different operating circumstances, the efficacy of the proposed battery charger is verified. Additionally, the input to the battery charger is regarded to be an AC power source with *230 V* RMS voltage and *50 Hz* frequency. The designed charger's responsiveness is confirmed while variable grid voltage operations are obtained for three separate situations, taking into account the various operating

circumstances. Fig. 6.3 shows the normal operation of the grid, Fig. 6.5 shows a non-ideal grid in which harmonics are introduced known as weak grid operation and Fig. 6.7 shows the *10%* sag & swell in the grid voltage which is also a non-ideal case. The total behaviour of all three cases is shown and changes is seen in power factor, battery current, and SoC. The THD is calculated for every case and a comparison is done.

Particularly noteworthy are the simulation findings during the G2V operation under rated conditions shown in Figs. (6.3),(6.5),(6.7), and THD responses in Figs. (6.4),(6.6),(6.8). The waveforms of in-phase grid voltage, Vg, and grid current, Ig, illustrated in Fig. 6.3, indicate unity-power-factor (UPF) charging. Furthermore, the stabilized DC link voltage, Vdc, validates the VSC's efficacy. Additionally, Ibat's controlled charging current demonstrates that the created charger efficiently controls the charging activity. Also, the battery current ripples adhere to the pertinent international standard. Fig. 6.4 also shows the fast Fourier-transform (FFT) evaluation of the grid current. The total harmonics distortion (THD) of grid current is indicated as *1.61%* here. As a result, the designed charger's G2V functioning adheres to the power quality requirement, and the battery is being charged.

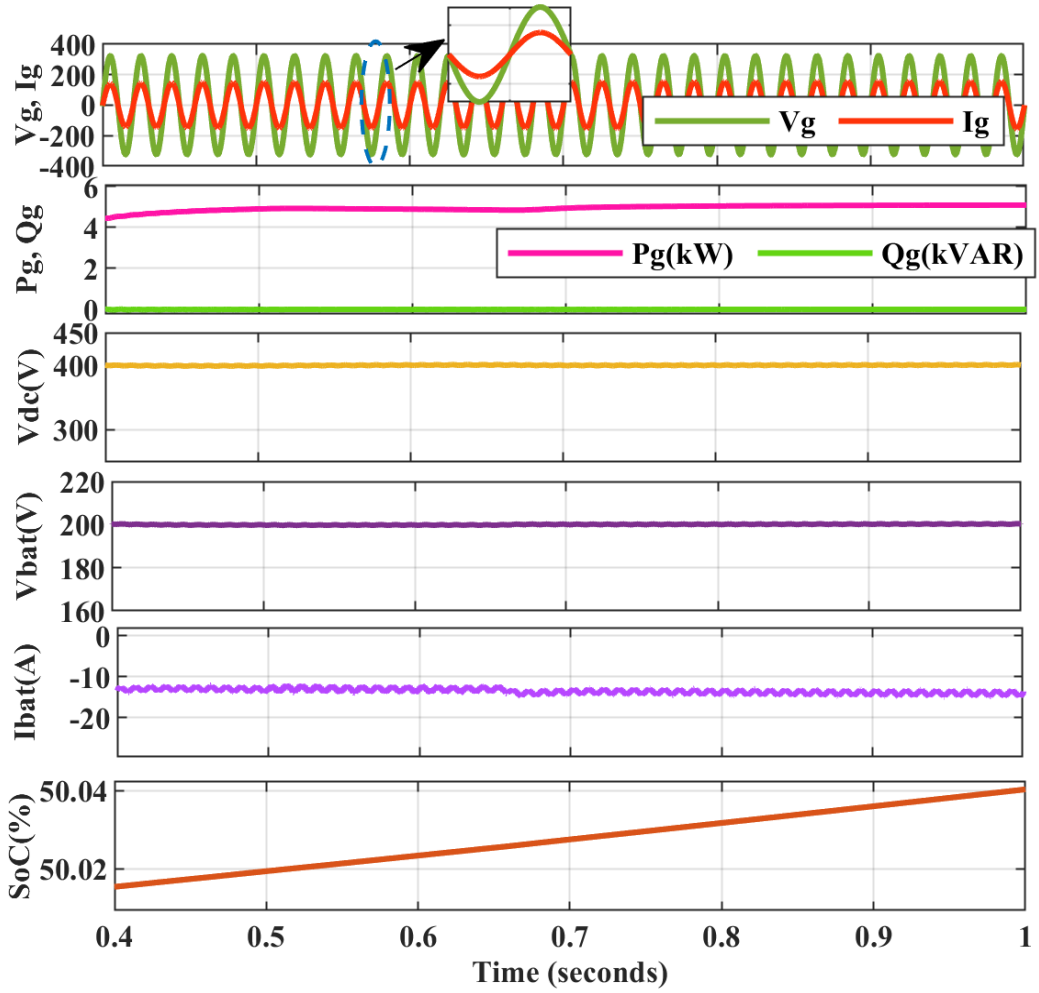

Fig. 6.3. Steady state performance under normal operating condition.

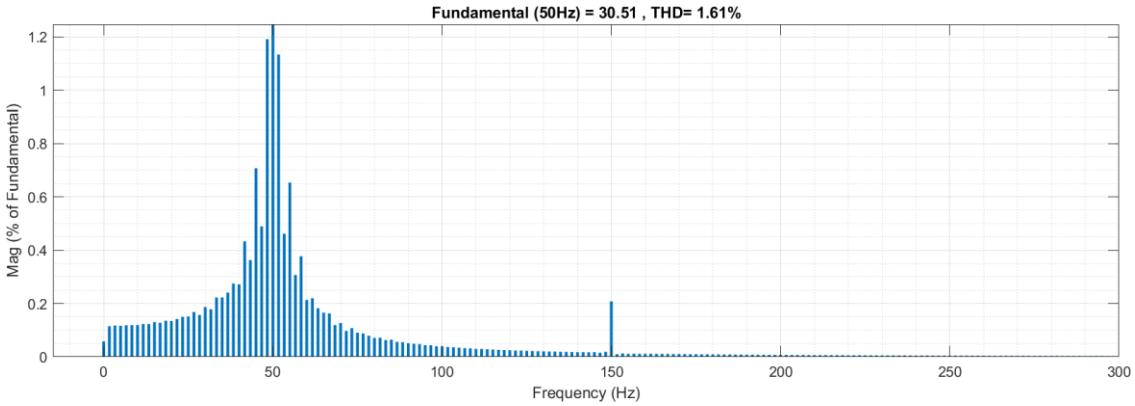

Fig. 6.4. THD under normal operating condition.

Fig. 6.5 depicts the system's weak grid operation, in which odd-ordered harmonics are added to grid voltage to test the system's robustness. As illustrated in Fig. 6.5, odd-ordered harmonics such as the 5^{th}, 7^{th}, 11^{th}, and 13^{th} distort the grid voltage, but an input filter with SOGI control is far more efficient, attempting to align grid current with grid voltage to preserve power factor. V_{dc} and the battery charging current are both constant during this procedure. The predicted THD for this operation is *2.02%*, which is likewise following the IEC requirement for grid current, as shown in Fig. 6.6.

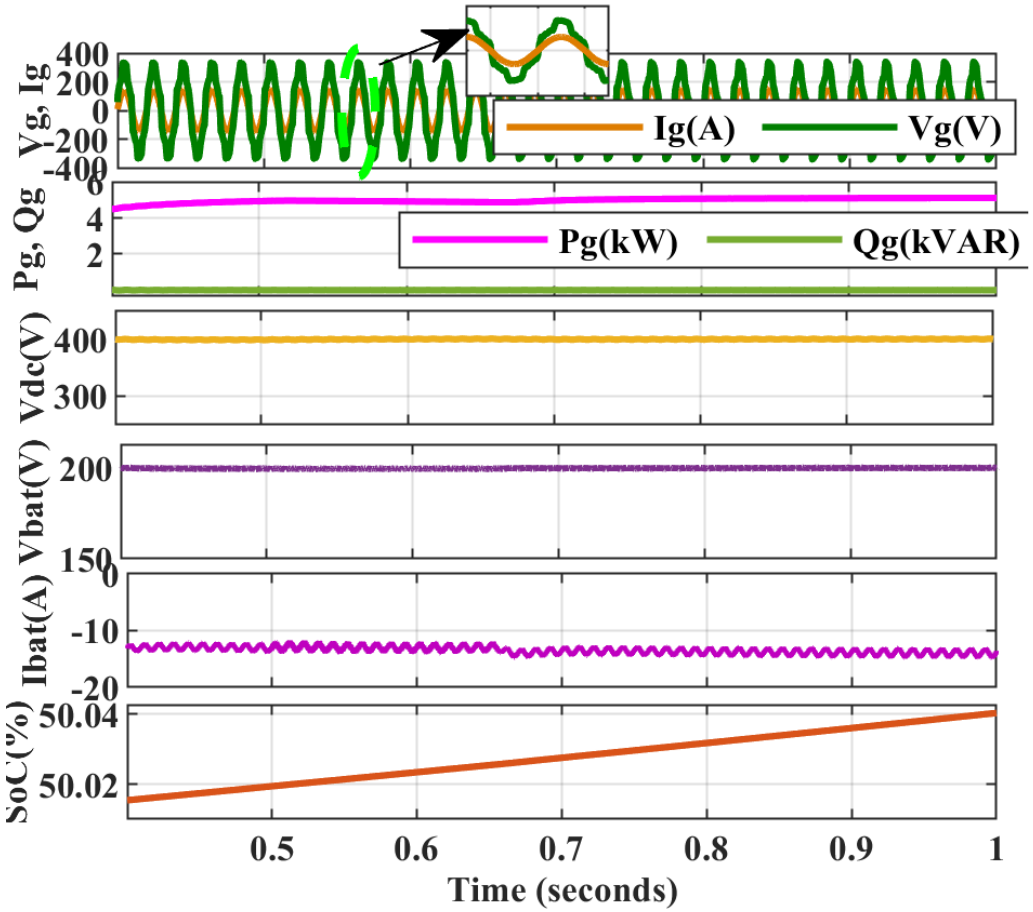

Fig. 6.5. Steady state performance when harmonics are injected (weak grid operating condition).

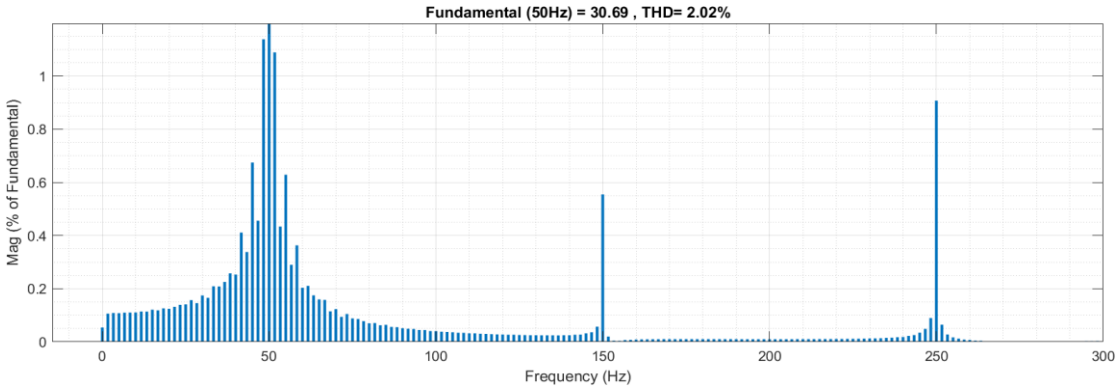

Fig. 6.6. THD under weak grid operation.

Fig. 6.5 depicts the sag and swell of grid voltage under non-ideal conditions. During this operation, 10% of grid voltage is reduced between *0.5s* and *0.6s,* and *10%* of grid voltage is increased between 0.7s and 0.8s, demonstrating the system's durability as V_{dc} is maintained constant throughout the operation, battery charging current is also kept constant. Notably, THD adheres to the IEC norm for grid current quality, which is *1.87%* in this situation, as seen in Fig. 6.8.

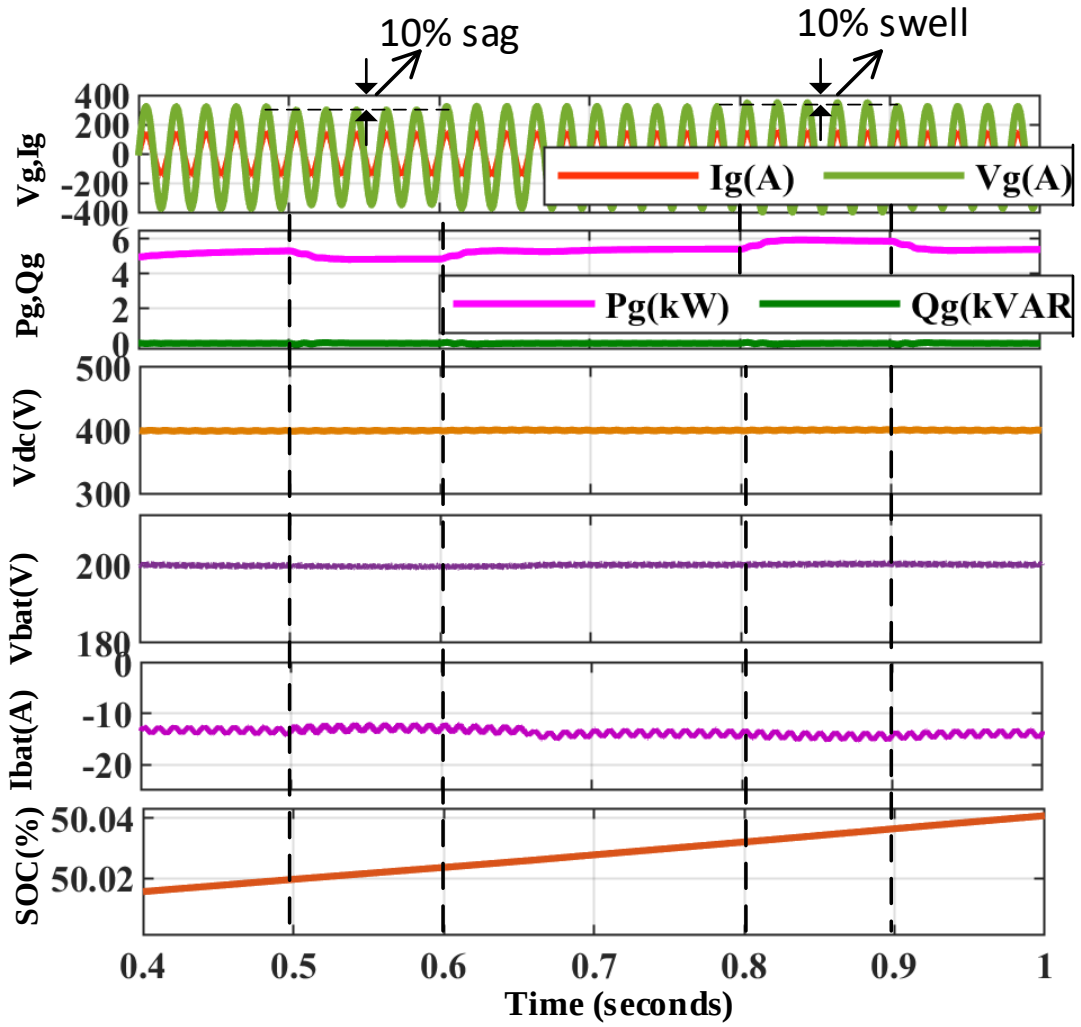

Fig. 6.7. Steady state performance when sag and swell in grid voltage.

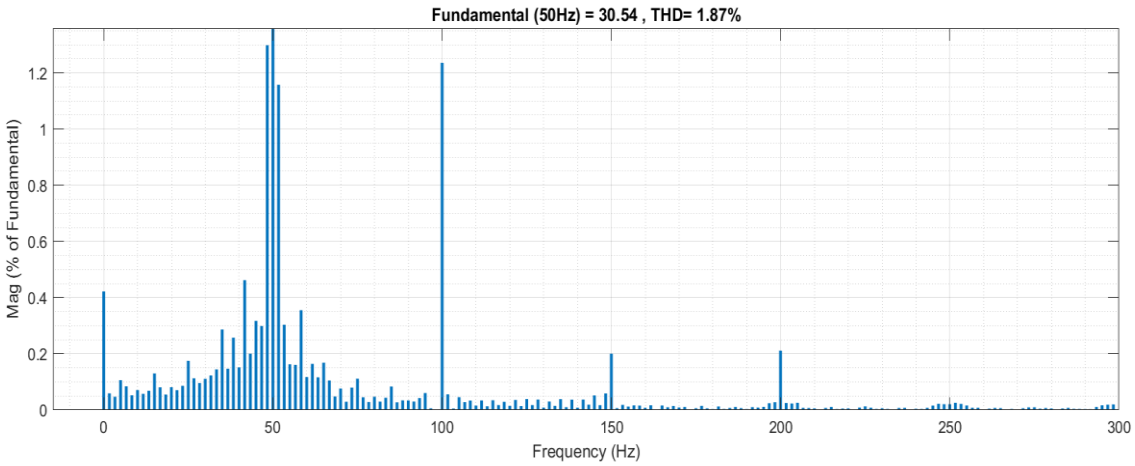

Fig. 6.8. THD under sag-swell voltage variation.

The resonating behaviour of the regulated MOSFET switches is seen in Fig. 6.9. To boost system efficiency with significantly reduced losses in the DC-DC conversion

stage, all switches achieve ZVS at all conditions during G2V operating mode. All of the switches dissipate close to zero power for the Modified LLC converter, which justifies the need for isolated converters in the system nicely.

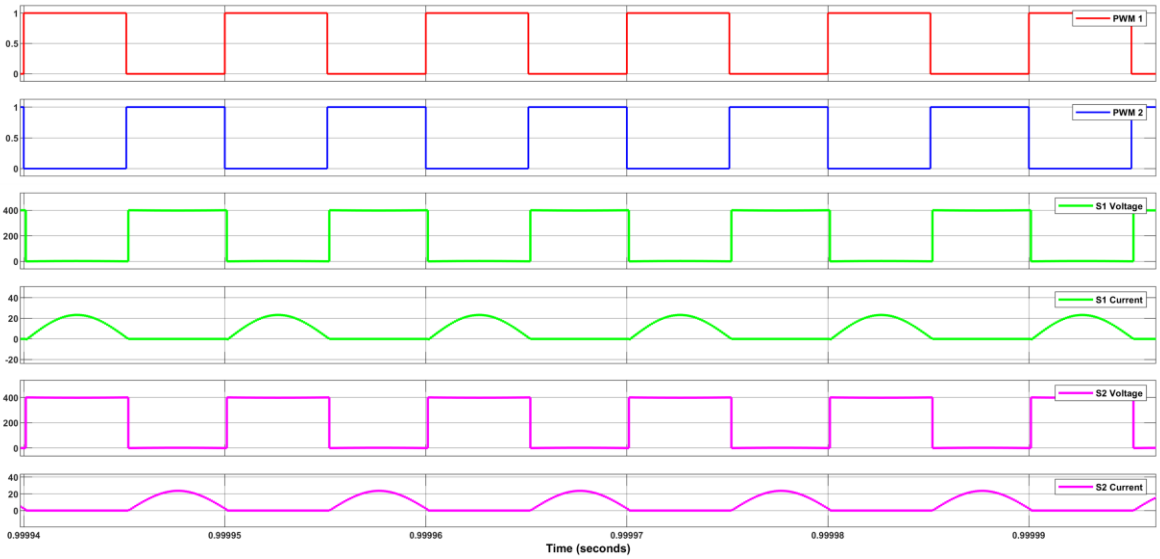

Fig. 6.9. Resonating nature of switches showing voltage and current with respect to the PWM.

Chapter 7

CONCLUSION AND FUTURE SCOPE

An onboard electric car battery charger with one phase and two stages is built and modeled in the MATLAB Simulink framework. Initial design and simulation of the Modified LLC resonant converter take place at resonance frequency as well as frequencies above and below resonance frequency. The improved LLC resonant converter has been shown to improve performance close to the resonance frequency. Additionally, the SOGI controller with input filter power factor correction is combined with the modified LLC resonant converter to increase the power quality of the AC supply current with a maximum THD of 2.02%, as shown in Chapter 5. Two converters are introduced with a controlled scheme separately. AC-DC converter is controlled through a SOGI controller whereas a modified DC-DC converter is controlled through a PI controller and optimum results are obtained for diverse conditions. The functionality of the suggested technique is demonstrated by Matlab/Simulink results. Grid to Vehicle charging mode is designed for onboard EV chargers. At a frequency switching of 100 kHz, the onboard charger's planned system architecture was realized. The final findings demonstrate that the specified power efficiency is greater than 96%, the PF is over 99%, and the THD of grid current is less than 2% for the three separate situations described above. To demonstrate the reliability and efficiency of the SOGI controller for AC-DC converters and the PI controller for modified DC-DC converters, simulation studies are performed as well under steady state and dynamic conditions. For large voltage, large power EV charging applications, the LLC single phase On-Board charger offers inexpensive pricing, minimal electromagnetic interference, excellent dependability, compactness, and highly effective development. To assure converter performance within a wide voltage range for EV charging applications, a modified LLC converter's resonant behaviour is discovered inside the operational region using a second-order generalized integrated approach.

Future experimental testing will be conducted to obtain a more precise picture of the overall effectiveness of your suggested system. For the DC-DC converter, a more durable and effective controller will be used to stabilize the dynamic behaviour of the

battery side. The power factor correction circuit will allow the prototype form of the Half-Bridge LLC resonant converter to be commercialized in the future.

REFERENCES

[1]. Nicoletti, L.; Bronner, M.; Danquah, B.; Koch, A.; Konig, A.; Krapf, S.; Pathak, A.; Schockenhoff, F.; Sethuraman, G.; Wolff, S.; et al. Review of trends and potentials in the vehicle concept development process. In Proceedings of the 2020 Fifteenth International Conference on Ecological Vehicles and Renewable Energies (EVER), Monte-Carlo, Monaco, 10–12 September 2020; pp. 1–5, ISBN 978-1-7281-5641-5.

[2]. Trommer, S.; Kolarova, V.; Fraedrich, E.; Kröger, L.; Kickhöfer, B.; Kuhnimhof, T.; Lenz, B.; Phleps, P. Autonomous Driving. The Impact of Vehicle Automation on Mobility Behavior; Institute for Mobility Research: Munich, Germany, 2016. Available online: https://www.researchgate.net/publication/312374304_Autonomous_Driving_-_The_Impact_of_Vehicle_Automation_ on_Mobility_Behaviour (accessed on 20 December 2020).

[3]. Nicoletti, L.; Romano, A.; König, A.; Schockenhoff, F.; Lienkamp, M. Parametric Modeling of Mass and Volume Effects for Battery Electric Vehicles, with Focus on the Wheel Components. WEVJ 2020, 11, 63.

[4]. H. A. Attar, M. Ghanes, M. Hamida and M. Taleb, "Control strategies design and comparison of DC-DC LLC converter in V2X mode for electric vehicle charger application," in 2021 IEEE Conference on Control Technology and Applications (CCTA), San Diego, CA, USA, 2021.

[5]. S. Mittal, A. Singh and P. Chittora, "EV Control in G2V and V2G modes using SOGI Controller," in 2022 IEEE 3rd Global Conference for Advancement in Technology (GCAT), 2022.

[6]. H. Li, Z. Zhang, S. Wang, J. Tang, X. Ren and Q. Chen, "A 300-kHz 6.6-kW SiC Bidirectional LLC Onboard Charger," IEEE Transactions on Industrial Electronics, vol. 67, no. 2, pp. 1435-1445, 2020.

[7]. The state of play in electric vehicle charging services – A review of infrastructure provision, players, and policies

[8]. X. Chen, G. Xu, X. Shiming , H. Han, M. Su, Y. Sun, H. Wang, Y. Liu and W. Xiong, "A Natural Bidirectional Input-Series–Output-Parallel LLC-DCX Converter With Automatic Power Sharing and Power Limitation Capability for Li-Ion Battery Formation and Grading System," IEEE Journal of Emerging and Selected Topics in Power Electronics, vol. 8, no. 4, pp. 3618-3632, 2020.

[9]. J. Zhang, J. Liu, J. Yang, N. Zhao, Y. Wang and T. Q. Zheng, "An LLC-LC Type Bidirectional Control Strategy for an LLC Resonant Converter in Power Electronic Traction Transformer," IEEE Transactions on Industrial Electronics, vol. 65, no. 11, pp. 8595-8604, 2018.

[10]. Z. U. Zahid, Z. M. Dalala, R. Chen, B. Chen and J. Lai, "Design of Bidirectional DC–DC Resonant Converter for Vehicle-to-Grid (V2G) Applications," IEEE Transactions on Transportation Electrification 1, vol. 1, pp. 232-244, 2015.

[11]. P. He and A. Khaligh, "Comprehensive Analyses and Comparison of 1 kW Isolated DC–DC Converters for Bidirectional EV Charging Systems," IEEE Transactions on Transportation Electrification, vol. 3, no. 1, pp. 147-156, 2017.
[12]. T. Jiang, J. Zhang, X. Wu, K. Sheng and Y. Wang , "A Bidirectional LLC Resonant Converter With Automatic Forward and Backward Mode Transition," IEEE Transactions on Power Electronics, vol. 30, pp. 757-770, 2015.
[13]. C. Wang, S. h. Zhang, . Y.-f. Wang, B. Chen and J.-h. Liu, "A 5-kW Isolated High Voltage Conversion Ratio Bidirectional CLTC Resonant DC–DC Converter With Wide Gain Range and High Efficiency," IEEE Transactions on Power Electronics, vol. 34, pp. 340-355, 2019.
[14]. S. Wenjin, X. Yan, W. Hongfei and D. Jie, "Modified High-Efficiency LLC Converters With Two Split Resonant Branches for Wide Input-Voltage Range Applications," IEEE Transactions on Power Electronics, vol. 33, no. 9, pp. 7867-7879, 2018.
[15]. S. Tong, R. Xiaoyong, C. Qianhong, Z. Zhiliang and R. Xinbo, "Reliability and efficiency improvement in LLC resonant converter by adopting GaN transistor," in 2015 IEEE Applied Power Electronics Conference and Exposition (APEC), 2015, pp. 2459-2463.
[16]. K. Seth and M. Singh, "Unified adaptive neuro-fuzzy inference system control for OFF board electric vehicle charger," International Journal of Electrical Power & Energy Systems, vol. 130, no. 0142-0615, p. 106896, 2021.
[17]. K. Seth and M. Singh, "Second-Order Ripple Minimization in Single-Phase Single-Stage Onboard PEV Charger," IEEE Transactions on Transportation Electrification, vol. 7, no. 3, pp. 1186-1195, 2021.
[18]. J. Zhang, J. Liu, J. Yang, N. Zhao, Y. Wang and T. Q. Zheng, "An LLC-LC Type Bidirectional Control Strategy for an LLC Resonant Converter in Power Electronic Traction Transformer".
[19]. X. Chen, G. Xu, X. Shiming , H. Han, M. Su, Y. Sun, H. Wang, Y. Liu and W. Xiong, "A Natural Bidirectional Input-Series–Output-Parallel LLC-DCX Converter With Automatic Power Sharing and Power Limitation Capability for Li-Ion Battery Formation and Grading System," IEEE Journal of Emerging and Selected Topics in Power Electronics, vol. 8, no. 4, pp. 3618-3632, 2020.
[20]. S. Md, M. T. Elrais, S. Ghosh, R. Rezaii and I. Batarseh, "A Comprehensive Review of Power Converter Topologies and Control Methods for Electric Vehicle Fast Charging Applications," IEEE Access, vol. 10, pp. 40753-40793, 2022.
[21]. S. LaMonaca and L. Ryan, "The state of play in electric vehicle charging services – A review of infrastructure provision, players, and policies," Renewable and Sustainable Energy Reviews, vol. 154, p. 111733, 2022.
[22]. K. Aswini, J. Kamala, L. Sriram, B. Kowshik, B. R. Vara Prasad and D. V. Sai Bharani, "Design and Analysis of Bidirectional Battery Charger for Electric Vehicle," INTERNATIONAL JOURNAL OF ENGINEERING RESEARCH & TECHNOLOGY (IJERT), vol. 10, no. 7, 2021.
[23]. S. Chakraborty, H.-N. Vu, M. M. Hasan, D.-D. Tran, M. E. Baghdadi and O. Hegazy, "DC-DC Converter Topologies for Electric Vehicles, Plug-in Hybrid

Electric Vehicles and Fast Charging Stations: State of the Art and Future Trends," Energies, vol. 12, no. 8, pp. 1-43, April 2019.

[24]. M. Xiaochen, W. Ping, B. Hukan and W. Zhishuang, "A Bidirectional LLCL Resonant DC-DC Converter With Reduced Resonant Tank Currents and Reduced Voltage Stress of the Resonant Capacitor," IEEE Access, vol. 8, pp. 125549-125564, 2020.

[25]. Singh, B. N. Singh, A. Chandra, K. Al-Haddad, A. Pandey and D. P. Kothari, "A review of three-phase improved power quality AC-DC converters," IEEE Transactions on Industrial Electronics, vol. 51, no. 3, pp. 641-660, 2004.

[26]. H. Yap, R. M. A. Mohd, H. M. Khair and M. N. Farzilah, "Operation of Three-Level Inverter-Based Shunt Active Power Filter Under Nonideal Grid Voltage Conditions With Dual Fundamental Component Extraction," IEEE Transactions on Power Electronics, vol. 33, no. 9, pp. 7558-7570, 2018.

[27]. S. Chalia, A. K. Seth and M. Singh, "Electric Vehicle Charging Standards in India and Safety Consideration," 2021 IEEE 8th Uttar Pradesh Section International Conference on Electrical, Electronics and Computer Engineering (UPCON), Dehradun, India, 2021, pp. 1-6, doi: 10.1109/UPCON52273.2021.9667649.

[28]. Wang, S. Zhang, Y. Wang, B. Chen, and J. Liu, “A 5-kW isolated high voltage conversion ratio bidirectional CLTC resonant DC–DC converter with wide gain range and high efficiency,” IEEE Trans. Power Electron., vol. 34, no. 1, pp. 340–355, Jan. 2019.

[29]. N. Z. Kashani, M. A. Parazdeh, M. Eldoromi, A. A. M. Birjandi and P. Amiri, "Grid Synchronization of Bidirectional Electric Vehicle Chargers Using Second Order Generalized Integrator based Phase Lock Loop," 2021 12th Power Electronics, Drive Systems, and Technologies Conference (PEDSTC), Tabriz, Iran, 2021, pp. 1-5, doi: 10.1109/PEDSTC52094.2021.9405867.

[30]. J. Zeng, G. Zhang, S. S. Yu, B. Zhang and Y. Zhang, "LLC resonant converter topologies and industrial applications — A review," in Chinese Journal of Electrical Engineering, vol. 6, no. 3, pp. 73-84, Sept. 2020, doi: 10.23919/CJEE.2020.000021.

[31]. P. He and A. Khaligh, "Comprehensive Analyses and Comparison of 1 kW Isolated DC–DC Converters for Bidirectional EV Charging Systems," in IEEE Transactions on Transportation Electrification, vol. 3, no. 1, pp. 147-156, March 2017, doi: 10.1109/TTE.2016.2630927.

[32]. H. Li, Z. Zhang, S. Wang, J. Tang, X. Ren and Q. Chen, "A 300-kHz 6.6-kW SiC Bidirectional LLC Onboard Charger," in IEEE Transactions on Industrial Electronics, vol. 67, no. 2, pp. 1435-1445, Feb. 2020, doi: 10.1109/TIE.2019.2910048.

[33]. Z. Zhang, Y.-Q. Wu, D.-J. Gu, and Q. Chen, “Current ripple mechanism with quantization in digital LLC converters for battery charging applications,” IEEE Trans. Power Electron., vol. 33, no. 2, pp. 1303–1312, Feb. 2018.

[34]. Z. U. Zahid, Z. M. Dalala, R. Chen, B. Chen, and J.-S. Lai, “Design of bidirectional DC–DC resonant converter for vehicle-to-grid (V2G)

applications," IEEE Trans. Transp. Electrific., vol. 1, no. 3, pp. 232–244, Oct. 2015.
[35]. M. Safayatullah, M. T. Elrais, S. Ghosh, R. Rezaii and I. Batarseh, "A Comprehensive Review of Power Converter Topologies and Control Methods for Electric Vehicle Fast Charging Applications," in IEEE Access, vol. 10, pp. 40753-40793, 2022, doi: 10.1109/ACCESS.2022.3166935.
[36]. G. Krishna, ''Understanding and identifying barriers to electric vehicle adoption through thematic analysis,'' Transp. Res. Interdiscipl. Perspect., vol. 10, pp. 1–9, Apr. 2021.
[37]. H. F. Farahani, A. Rabiee, and M. Khalili, ''Plug-in electric vehicles as a harmonic compensator into microgrids,'' J. Cleaner Prod., vol. 159, pp. 388–396, Aug. 2017.
[38]. Khaligh and M. D'Antonio, ''Global trends in high-power on-board chargers for electric vehicles,'' IEEE Trans. Veh. Technol., vol. 68, no. 4, pp. 3306–3324, Apr. 2019.
[39]. Wang, X. Qu, Y. Yao, and P. Yang, ''Hybrid inductive-power-transfer battery chargers for electric vehicle onboard charging with configurable charging profile,'' IEEE Trans. Intell. Transp. Syst., vol. 22, no. 1, pp. 592–599, Jan. 2021.
[40]. S. A. Arshadi, M. Ordonez, W. Eberle, M. Craciun, and C. Botting, "Three-phase LLC battery charger: Wide regulation and improved light-load operation," IEEE Trans. Power Electron, vol. 36, pp. 1519–1531, 2020.
[41]. N. Altin, S. Ozdemir, M. Khayamy and A. Nasiri, "A Novel Topology for Solar PV Inverter Based on an LLC Resonant Converter With Optimal Frequency and Phase-Shift Control," in *IEEE Transactions on Industry Applications*, vol. 58, no. 4, pp. 5042-5054, July-Aug. 2022, doi: 10.1109/TIA.2022.3163372.
[42]. Q. Zhao, J. Zhang, Y. Gao, D. Wang and Q. Yang, "Hybrid Variable Frequency LLC Resonant Converter with Wide Output Voltage Range," in *IEEE Transactions on Power Electronics*, doi: 10.1109/TPEL.2023.3283548.
[43]. J. Wu, S. Li, S. -C. Tan and S. Y. R. Hui, "Frequency Folding for LLC Resonant Converters in EV Charging Applications," in *IEEE Transactions on Power Electronics*, vol. 38, no. 4, pp. 5041-5054, April 2023, doi: 10.1109/TPEL.2023.3235114.
[44]. Zhangyong Chen, Xintong Zhu, Gen Chen, Yong Chen, Chenchen Feng, Frequency-adapted hybrid modulation strategy of resonant converter with narrow frequency range, International Journal of Circuit Theory and Applications, 10.1002/cta.3621, (2023).
[45]. R. K. Lenka, A. K. Panda, A. R. Dash, L. Senapati and N. Tiwary, "A Unified Control of Grid-Interactive Off-Board EV Battery Charger With Improved Power Quality," in *IEEE Transactions on Transportation Electrification*, vol. 9, no. 1, pp. 920-933, March 2023, doi: 10.1109/TTE.2022.3172354.

LIST OF PUBLICATIONS

- M Ansari, G. Yadav, M. Singh, "Modified Bidirectional LLC Converter for Electric Vehicle Application." in *IEEE Conference, 2023 Second International Conference on Electrical, Electronics, Information and Communication Technologies (ICEEICT 2023)*, **(Presented).**
- M Ansari, G. Yadav, M. Singh, "A 3.3kW Modified LLC Resonant Converter for Grid-Tied EV System Under Wide Voltage Range." in *IEEE Conference 3rd CONIT*, **(Accepted).**

2023 Second International Conference on

Electrical, Electronics, Information and Communication Technologies (ICEEICT 2023)

05 - 07, April 2023 | Trichy, Tamil Nadu, India | www.iceict.in

CERTIFICATE

Sponsored by

IEEE
Advancing Technology for Humanity

EE 2043
Peer Reviewed

This certificate is presented to

Monish Ansari
Electrical Engineering Department
Delhi Technological University
Delhi, India

for presenting the research paper entitled "Modified Bidirectional LLC Converter for Electric Vehicle Application" in the IEEE sponsored Second International Conference on Electrical, Electronics, Information and Communication Technologies (ICEEICT 2023) organized by the Department of Electrical and Electronics Engineering, K. Ramakrishnan College of Engineering, Tiruchirappalli, Tamil Nadu, India during 05 – 07, April 2023.

Dr. K. Dhayalini
Conference Chair

Dr. D. Srinivasan
General Chair

Organized by

Department of Electrical and Electronics Engineering
K. Ramakrishnan College of Engineering
Trichy, Tamil Nadu, INDIA

Promotional Partner
DILIGENTEC SOLUTIONS

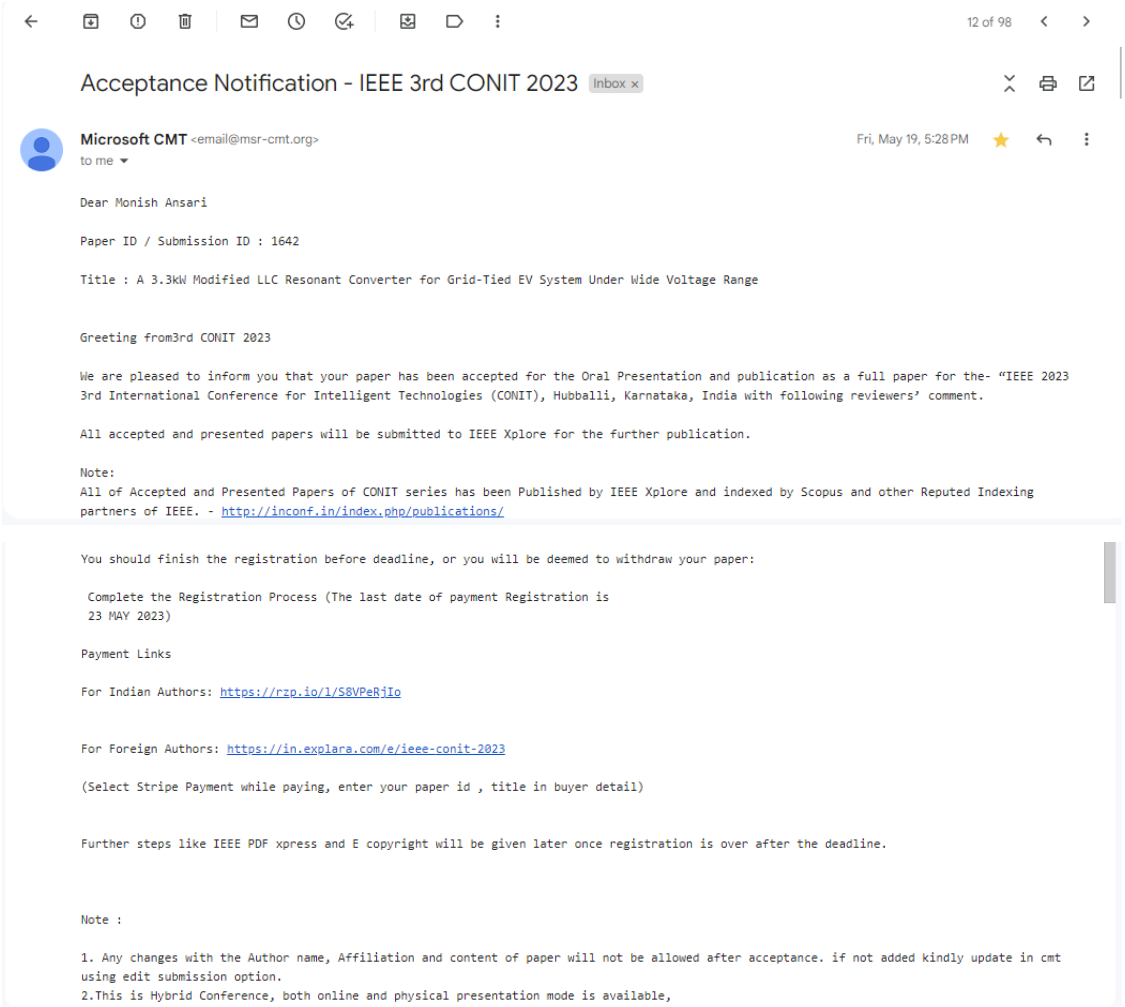

12 of 98

Acceptance Notification - IEEE 3rd CONIT 2023 Inbox ×

Microsoft CMT <email@msr-cmt.org> Fri, May 19, 5:28 PM

to me

Dear Monish Ansari

Paper ID / Submission ID : 1642

Title : A 3.3kW Modified LLC Resonant Converter for Grid-Tied EV System Under Wide Voltage Range

Greeting from3rd CONIT 2023

We are pleased to inform you that your paper has been accepted for the Oral Presentation and publication as a full paper for the- "IEEE 2023 3rd International Conference for Intelligent Technologies (CONIT), Hubballi, Karnataka, India with following reviewers' comment.

All accepted and presented papers will be submitted to IEEE Xplore for the further publication.

Note:
All of Accepted and Presented Papers of CONIT series has been Published by IEEE Xplore and indexed by Scopus and other Reputed Indexing partners of IEEE. - http://inconf.in/index.php/publications/

You should finish the registration before deadline, or you will be deemed to withdraw your paper:

Complete the Registration Process (The last date of payment Registration is 23 MAY 2023)

Payment Links

For Indian Authors: https://rzp.io/l/S8VPeRjIo

For Foreign Authors: https://in.explara.com/e/ieee-conit-2023

(Select Stripe Payment while paying, enter your paper id , title in buyer detail)

Further steps like IEEE PDF xpress and E copyright will be given later once registration is over after the deadline.

Note :

1. Any changes with the Author name, Affiliation and content of paper will not be allowed after acceptance. if not added kindly update in cmt using edit submission option.
2.This is Hybrid Conference, both online and physical presentation mode is available,